Volume V - The Performance:

Analysis of the London Avenue Canal I-wall Breaches

Executive Summary

This interim IPET report describes detailed assessments of the two breaches that occurred at the London Avenue Canal. The investigation of these breaches is an important step in IPET's system-wide investigation of floodwall and levee performance, and the findings illuminate a possible mechanism of failure that will be investigated system-wide for locations where sand underlies levees and floodwalls.

The breach on the London Avenue Canal near Mirabeau Avenue (the south breach) occurred at 6:00 AM to 7:00 AM on Monday, 29 August 2005. The breach on the London Avenue Canal near Robert E. Lee Boulevard (the north breach) occurred about an hour later. Field evidence, analyses, and physical model tests show that the breaches were due to the effects of high water pressures within the sand layer beneath the levee, and high water loads on the walls. The London Avenue Canal breaches had a key factor in common with the 17th Street Canal breach – formation of a gap between the wall and the levee fill on the canal side of the wall. At both the 17th Street Canal and the London Avenue Canal, formation of a gap allowed high water pressures to act on the wall below the surface of the levee, severely loading the wall. At the London Avenue Canal, an additional effect of the gap was that water flowed down through the gap into the underlying sand. High water pressures in the sand uplifted the marsh layer on the landside of the levee, resulting in concentrated flow and erosion, removing material and reducing support for the floodwall.

Analyses of the south breach showed that erosion is the most likely principal mode of failure, with sliding instability occurring after significant volumes of sand and marsh had been removed by erosion and piping. Without alteration of the south breach cross section by erosion and piping on the landside of the levee, the calculated factors of safety with respect to sliding instability are greater than 1.0, indicating that alteration of the cross section by erosion and piping probably played an essential role in the failure at this location.

Field observations at the north breach indicate that the canal-side levee crest remained intact after the breach, and a playhouse on the property adjacent to the breach was heaved upward during the breach. The analyses presented in this report show that conditions for erosion and piping were present at the north breach, but the more likely cause of the failure was sliding instability. High uplift pressures likely resulted in a rupture through the marsh layer and the underlying thin layer of clay. At this location, however, the high pore pressures within the sand would reduce passive resistance sufficiently to result in sliding instability without significant alteration of the cross section.

FINAL DRAFT April 24, 2006

Analysis of the London Avenue Canal I-wall Breaches

Observations

Two I-wall failures resulting in breaches occurred at the London Avenue Canal during Hurricane Katrina, one on the east side of the canal at Mirabeau Avenue (the south breach), and the other on the west side of the canal at Robert E. Lee Boulevard (the north breach). At both locations the levees and I-walls were founded on a layer of marsh (peat) overlying sand.

The south breach, shown in Figure 1, occurred about 6:00 AM to 7:00 AM on August 29th, when the water level in the canal was 7.1 ft to 8.2 ft NAVD88. The breach was narrower than the breach at 17th Street and the London Avenue north breach. A deep scour hole formed due to the inrush of water, and a large amount of eroded sand was deposited in the neighborhood inland of the breach. It appears that the breach was quite narrow when it formed, and subsequently widened to about 60 ft as wall panels adjacent to the initial breach were undermined by scour, and tilted into the scour hole.

The north breach, shown in Figure 2, occurred about 7:00 AM to 8:00 AM on August 29th, about an hour after the south breach, when the canal water level was 8.2 ft to 9.5 ft NAVD88. The breach was about 410 ft wide, approximately the same width as the breach at 17th Street. A playhouse on the property adjacent to the breach was heaved upward when the breach occurred, indicating upward movement of the ground inboard of the levee toe. The I-wall opposite the north breach (on the east side of the canal) moved and tilted significantly at about the same time as the breach occurred on the west side, but the east I-wall did not breach. A line of sinkholes was observed at the inland side of the distressed east I-wall, and a sand boil at the inboard embankment toe indicate that erosive seepage and piping had occurred beneath the levee.

Possible Modes of Failure

At both the south and north breach locations, it seems likely that underseepage and erosion caused or contributed to the failures.

It is not possible to establish the cause of the south breach with certainty based on the field observations made after the failure. The failed sections of the I-wall were not found, and large volumes of sand were moved by the inflow of water through the breach, covering the landscape. The failure might have resulted from underseepage erosion and piping, or from sliding instability aggravated by seepage and uplift pressures. Analyses have been performed to examine both of these possibilities.

It has been reported that cold-rolled sheetpiles were used for the I-wall in the area of the south breach. Cold-rolled sheetpiles have lower interlock strengths than hot-rolled sheetpiles. Consequently, use of cold-rolled sheetpiles increases the likelihood that interlocks could have failed during driving, particularly because the sand in the south breach area was dense, and driving was hard. Interlock failure would result in gaps between adjacent sheets in the sheetpile wall, making it possible for water to seep through the wall as well as under the wall. Such through-flow would result in more severe seepage conditions than those reflected in the seepage

analyses described here, and would make erosion and piping an even more likely mode of failure at the south breach.

Field observations at the north breach indicate that sliding instability was likely the primary mode of failure, with seepage and high pore pressures in the sand as a significant contributing factor. It seems likely that the failure and breach were the result of insufficient passive resistance to counteract the water pressure forces to which the wall was subjected. The passive resistance was likely reduced by the effects of water seeping through the foundation soils beneath the levee and the marsh layer inland, inducing uplift pressures and reducing shear strengths. Analyses have been performed to examine the likelihood of erosion and piping, and instability due to uplift and reduced shear resistance.

London South Breach Seepage and Stability Analyses

Erosion and Piping

Finite element analyses of seepage beneath the I-wall were performed using the computer program SLIDE[1]. The characteristics of the cross section analyzed are shown in Figure 3. The relevant materials are the sand at the base of the section, the overlying marsh (peat) layer, and the clayey levee fill. The permeability of the sand, based on field pumping tests, was 1.5×10^{-2} cm/sec. The permeability of the marsh layer was estimated as 1×10^{-5} cm/sec, and the permeability of the levee fill and the Bay Sound clay was estimated as 1×10^{-6} cm/sec. Thorough analyses of transient and steady seepage, described in a separate report, indicated that (a) steady seepage through the sand was established quickly, and (b) the pore pressures within the sand and the uplift pressures on the base of the marsh layer are not affected by the permeability values assigned to the marsh layer and the levee fill, provided that those materials are at least two orders of magnitude less permeable than the sand. The values of permeability of the marsh layer and the levee fill used in the seepage analyses described here were selected in accordance with these findings, and are considered to be reasonable estimates of the permeabilities of these materials.

The hydraulic boundary conditions used in these analyses are shown in Figure 3. The canal water level was either 7.1 ft or 8.2 ft NAVD88, a range consistent with the estimated canal water levels at the time of failure. A constant-head boundary condition was imposed at the location of the drain beneath Warrington Drive. This head value was either -8.4 ft (the normal ground water level with pumps operating), or -5.1 ft NAVD88 (a higher level equal to the ground surface elevation, which might have occurred with pumps not operating). Reports indicate that the pumps stopped operating when the wall failed, severing the power line. In all, four different seepage cases were analyzed, as shown in Table 1.

Based on the study of the 17th Street Canal breach, it seems likely that a crack would form between the I-wall and the levee fill on the canal side of the wall. The type of crack assumed to have formed behind the 17th Street Canal I-wall, shown in Figure 4, does not seem feasible for the London Avenue foundation conditions, where the I-wall is driven into sand, because cohesionless sand would be unable to support a crack. A more likely condition for a wall driven into sand is shown in Figure 5. This “half-cracked” condition involves a crack through the levee fill and the marsh layer, down to the top of the sand. Water would fill this crack, loading the wall and introducing the canal head at the top of the sand. The part of the wall embedded in the

[1] Available from Rocscience Inc., 31 Balsam Avenue, Toronto, Ontario, Canada M4E 3B5

sand would be loaded by water pressures that are somewhat lower than hydrostatic pressures, plus active earth pressures, as shown in Figure 5. The lower-than-hydrostatic water pressures were determined from the finite element seepage analyses. All of the seepage and stability analyses were performed based on this half-cracked condition.

Six-node triangular elements were used for the seepage analyses. The finite element mesh is shown in Figure 6. Computed total head contours for Case 1 are shown in Figure 7. It can be seen that the flow through the sand is predominantly horizontal, and that the total head on the landward side of the levee is above the ground surface, which is at elevation –5.1 ft. The head contours for the other three cases shown in Table 1 had similar shapes, although the values varied somewhat depending on the canal water level and the Warrington Drive water level.

Computed pore pressures, or uplift pressures, at the base of the marsh layer are shown in Figure 8 for the four cases analyzed, together with the total overburden pressure at the base of the marsh layer. It can be seen that in all four cases the computed pore pressures exceed the total overburden pressure at the base of the marsh layer. This result indicates that the marsh layer would be heaved off the underlying sand by the high uplift water pressures. A likely result of this heave would be rupture of the marsh layer at one or more weak points, and upward flow of water through the rupture in the marsh material. This flow would relieve the high water pressure locally, and create a new hydraulic boundary condition at the point of rupture.

Additional seepage analyses were performed to determine if the hydraulic gradients within the sand after rupture of the marsh layer would be large enough to cause erosion of the sand and begin a piping failure. The seepage boundary conditions used in theses analyses are shown in Figure 9, where a rupture extends upward through the marsh layer, from the top of the sand to the ground surface. The hydraulic gradients computed in these analyses were found to depend on the assumed width of the rupture in the marsh layer. While it seems clear that the marsh layer would rupture when the uplift pressures exceeded the overburden pressures, the width of the rupture would depend on factors that cannot be evaluated, and it is thus necessary to assign a width to the rupture zone based on judgment. Even so, we believe that the analytical results that follow reflect the essential aspects of the situation. The results support the view that the London south breach developed as a result of erosion and piping.

The narrower the assumed rupture zone, the higher the computed hydraulic gradient at the top of the sand below the rupture, because flow converges toward the rupture, and the flow velocities increase near the rupture. This converging flow is shown by the total head contours in the sand near the rupture in Figure 10. A rupture zone width equal to 1.6 ft was used in the analyses, based on a judgment of what seemed a reasonable and possible rupture zone size. Doubling the width of the rupture zone was found to reduce the computed hydraulic gradient by 23%, and cutting the width in half increased the hydraulic gradient by 33%. In the real case, flow would converge in three dimensions rather than two dimensions, as represented in these two-dimensional seepage analyses. It therefore seems likely that the actual hydraulic gradients would be higher than the values discussed in the following sections, but the magnitude of this three-dimensional effect cannot be quantified.

The changed hydraulic boundary conditions caused by the rupture through the marsh layer were computed by imposing a head at the base of the rupture that was equal to the elevation of the ground surface, simulating a condition where the water level within the ruptured zone rises to the ground surface. Values of vertical hydraulic gradient at the top of the sand for this condition

are shown in Table 2 for the four cases analyzed. It can be seen that they range from 1.03 to 1.24.

The value of hydraulic gradient that would cause erosion of the sand is

$$i_{critical} = \frac{\gamma_b}{\gamma_w} = \frac{\gamma_s - \gamma_w}{\gamma_w}$$

where $i_{critical}$ = hydraulic gradient that would cause erosion of the sand, γ_b = buoyant unit weight of sand, γ_w = unit weight of water, and γ_s = saturated unit weight of sand. With γ_s for the sand assumed to be 120 pcf, the critical hydraulic gradient is 0.92. Thus the values of hydraulic gradient for all four cases analyzed would be large enough to cause erosion and to begin piping, as shown by the values of $F_{erosion}$ listed in Table 2.

Considering the variation in factor of safety caused by the uncertain landside water level, the probability of erosion was calculated as shown in Table 3. A simple method based on the Taylor series[2] was used for these calculations. It can be seen that the probability of erosion approaches 100% for both canal water levels, indicating a high likelihood that erosion occurred and that erosion was the cause of the failure, or an exacerbating factor in the failure.

Considering that three-dimensional concentration of flow would result in even larger hydraulic gradients, it appears that erosion and piping of the sand would be likely at the south breach. With high hydraulic gradients, backward erosion could occur rapidly, extending back to the I-wall, and leading to a catastrophic failure of the type that was observed. The analyses described here consider only the beginning of this process. Once erosion of the sand into the rupture in the marsh layer began, the situation would deteriorate quickly as seepage converged to the zone of erosion, and the rate of erosion increased. Eventually, after enough sand, marsh and possibly levee fill had been eroded away, an unstable condition would develop, with the passive resistance of the materials landward of the wall becoming too small to resist the forces of the water and earth pressures pushing from the canal side of the wall.

Slope Instability

While this erosion and piping failure mechanism appears plausible based on the results of the analyses described above, it is of interest also to examine the possibility that the failure could have occurred by sliding, through a slope instability failure mechanism. To examine this possibility, slope stability analyses were performed using the computer program SLIDE[1].

The stability analyses were performed for the cross section shown in Figures 11, 12, 13, and 14. This is the same cross section as used in the seepage analyses, and the same canal water levels and landside water levels were used.

Standard Penetration Tests performed in the breach area before the breach showed that the sand had Standard Penetration Test blow counts (N_{SPT}) greater than 50, which would correspond to values of ϕ' in the range of 40 degrees to 46 degrees. Cone penetration tests performed after the breach showed high tip resistance in the sand adjacent to the breach, which correspond to

[2] Wolff, T. F. (1994). "Evaluating the reliability of existing levees." Report, Research Project: Reliability of Existing Levees, prepared for U.S. Army Engineer Waterways Experiment Station Geotechnical Laboratory, Vicksburg, Miss.

similar values of ϕ'. In order not to overestimate the strength of the sand, a value of ϕ' = 40 degrees was used in the stability analyses.

The marsh was treated as undrained, with s_u = 300 psf, and ϕ_u = 0, based on the available test results. A value of s_u = 300 psf is considered appropriate for the areas beneath the canal-side levee slope and beyond the levee toe, where the slip circles pass through the marsh. The unit weight of the marsh was assumed to be 80 pcf.

The levee fill was also treated as undrained, with s_u = 900 psf, and ϕ_u = 0. The slip circles do not intersect the levee fill, however, and the levee strength therefore has no influence on the calculated values of factor of safety. The unit weight of the levee fill was assumed to be 109 pcf.

Analyses were performed with canal water levels at 7.1 ft and 8.2 ft NAVD88, using pore pressures in the sand from the finite element seepage analyses without a rupture through the marsh layer. The non-ruptured seepage analyses were used to determine pore pressures because the rupture is conceived as a feature of very limited size, not appropriate for inclusion in a two-dimensional cross section. At the bases of the slices where the pore pressures exceeded the overburden pressures near the top of the sand on the inboard side, zero shear strength was assigned for the sand.

As discussed earlier, it was assumed in all analyses that deflection of the wall toward the land side would result in formation of a crack through the levee fill and the marsh in back of the wall, down to the top of the sand. It was assumed that the crack would not extend into the sand, because the sand is cohesionless, and would be expected to slump and fill any gap. This "half-cracked" condition was used in all stability analyses. It can be seen in Figures 11, 12, 13, and 14 that the slip circles extend to the bottom of the sheetpile wall furthest from the canal.

The factors of safety calculated in these analyses are shown in Figures 11 through 14, and in Table 4. For the canal water levels estimated at the time of the breach (7.1 ft to 8.2 ft) the calculated factors of safety range from a low value of F = 1.19 to a high value of F = 1.56. Thus, with this interpretation of the available data, and consistent assumptions for the seepage and stability analyses, a mechanism of failure involving erosion and piping is plausible at the south breach, but a slope stability failure mechanism is not.

An analysis was performed, with the landside water level at -8.4 ft, to determine the canal water level corresponding to a calculated factor of safety equal to 1.00. As shown in Figure 15, a canal water level equal to 9.7 ft would be required for a factor of safety equal to 1.00. This is 1.5 ft higher than the highest estimated water level at the time the breach occurred, indicating that instability without removal of material by erosion and piping is unlikely at the south breach.

Additional stability analyses were performed, varying the friction angle of the sand and the strength of the marsh layer, to compute the probability of slope instability. The results of these cases are shown in Table 5. The Taylor series approach[2] was used to compute the standard deviation of the factor of safety and the probability of failure. The most likely value of factor of safety was taken as the average of the values for the high and low inland water levels. The probability of instability was estimated assuming a log-normal distribution of factor of safety, with the results shown in Table 5. It can be seen that the estimated probability of instability is 1% for the lower canal water level, and 10% for the higher canal water level. Thus, while there is a small probability that failure might have occurred due to instability without erosion and piping, this mode of failure is much less likely than failure by erosion and piping.

London North Breach Seepage and Stability Analyses

The possibilities of failure due to erosion and piping, and due to instability, were also examined for the London Avenue north breach. The differences between the London south breach analyses and the London north breach analyses were:

1. The seepage boundary conditions were different. The canal water level at the time of the north breach was 8.2 ft to 9.5 ft, higher than at the south breach because the north breach occurred later. The inland seepage boundary condition ranged from -8.4 ft to -3.9 ft because Pratt Drive is at a slightly higher elevation than Warrington Drive. Four cases were analyzed, using the seepage boundary conditions shown in Figure 16, and summarized Table 6. An additional analysis was performed to determine the canal water level required for a calculated factor of safety equal to 1.00.
2. The cross sections are somewhat different. On the inland side of the wall at the north breach, there is a thin layer of lacustrine clay between the marsh layer and the sand.
3. The sand is less dense in the north breach area. Standard Penetration Test blow counts (N_{SPT}) in this area range from 2 to 14, with an average of about 10. This range of values of N_{SPT} corresponds to values of ϕ' in the range of 30 degrees to 34 degrees. Cone penetration tests performed after the breach, in the area adjacent to the breach, showed tip resistances that correspond to about the same values of ϕ'. A value of ϕ' = 32 degrees was used in the stability analyses for the north breach area.

Erosion and Piping

Six-node triangular elements were used for the seepage analyses, as for the south breach. The finite element mesh for the north breach is shown in Figure 17. The same values of permeability were used as for the south breach. The lacustrine clay between the sand and the marsh layer was assumed to have a permeability of $1x10^{-6}$ cm/sec.

Computed total head contours for Case 1 are shown in Figure 18. As for the south breach, the flow through the sand is predominantly horizontal, and the total head on the landward side of the levee is above the ground surface, which is at elevation – 3.9 ft. The head contours for the other three cases that were analyzed had similar shapes, although the values varied somewhat depending on the canal water level and the Pratt Drive water level.

Water pressures at the base of the marsh layer for the north breach area are shown in Figure 19. As in the case of the south breach area, the uplift water pressures exceed the overburden pressures due to the weight of the marsh layer at the landside of the levee, and it would be expected that the marsh layer would be heaved upward and would rupture.

Additional seepage analyses were performed with revised boundary conditions, as was done in the south breach analyses, using the conditions shown in Figure 20. A rupture 1.6 ft wide, extending through the marsh layer and the lacustrine clay layer was assumed, and a hydraulic boundary condition with the water level at the ground surface was applied in the area of the rupture. Total head contours for the area around the assumed rupture through the lacustrine clay and peat are shown in Figure 21. The hydraulic gradients calculated for these conditions are shown in Table 7.

With γ_s for the sand equal to 115 pcf (5 pcf less than at the south breach where the sand was more dense), the critical hydraulic gradient is 0.84. The values of hydraulic gradient all four cases analyzed would be large enough to cause erosion and begin piping of the sand. Thus erosion and piping appears to be a plausible mode of failure for the London north breach, as well as the south breach.

Probabilities of erosion for the high and low canal water levels were calculated using the same procedure as for the south breach[2], with the results shown in Table 8. It can be seen that the probability of erosion exceeds 90% for both the low and the high canal water levels, and approaches 100% for the higher level. These probabilities are slightly smaller than for the south breach, where the probability of erosion approached 100% for both high and low canal water levels.

Slope Instability

While erosion and piping appears possible based on the results of the analyses described above, it is also of interest to examine the factor of safety against slope instability. To examine the possibility that the failure mechanism involved sliding, slope stability analyses were performed using the same procedures as used for the south breach. The stability analyses were performed for the cross section shown in Figures 22, 23, 24, and 25. This is the same cross section as used in the seepage analyses.

Analyses were performed for four cases, using the canal water levels and inland water levels shown in Table 6, and pore pressures in the sand from the same finite element seepage analyses used to compute the uplift pressures shown in Figure 19. As noted previously, a value of $\phi' = 32$ degrees was used for the sand. The strengths and unit weights of the marsh and the levee fill were the same as used in the south breach stability analyses described previously. The undrained strength of the lacustrine clay was assumed to be equal to 42 psf. The strength of this thin layer has a very small influence on the calculated factors of safety. At the bases of slices where the pore pressures exceeded the overburden pressures at the top of the sand on the inland side, zero shear strength was assigned for the sand.

The same half-cracked condition was used in these analyses as was used for stability analyses at the south breach. It can be seen in Figures 22, 23, 24, and 25 that the slip circles extend to the bottom of the sheetpiles. Full hydrostatic water pressure force acts on the sheetpile down to the top of the sand. From the top of the sand to the bottom of the sheetpile, the sheetpile is acted on by water pressures determined from the seepage analyses and active earth pressures.

The factors of safety for Cases 1 through 4 are shown in Figures 22 through 25, and are listed in Table 9. They range from a low value of F = 0.67 to a high value of F = 0.99. Thus, because the sand is considerably less dense in the north breach area, and would have a smaller friction angle, a mechanism of failure involving slope instability is plausible.

An additional analysis was performed, with the landside water level at -8.4 ft, to determine the canal water level corresponding to a calculated factor of safety equal to 1.00. As shown in Figure 26 and Table 9, a canal water level equal to 8.1 ft corresponds to a factor of safety equal to 1.00. This is very nearly equal to the lowest estimated water level at the time the breach occurred, indicating that instability is a highly likely mode of failure at the north breach.

Further analyses were performed, varying the friction angle of the sand and the strength of the marsh layer, to compute the probability of slope instability, using the Taylor series method[2]. The results of these cases are shown in Table 10. The most likely value of factor of safety was taken as the average of the values for the high and low inland water levels. The results of these calculations are shown in Table 10. It can be seen that the estimated probability of instability is 70% for the lower canal water level, and 97% for the higher canal water level. Thus, there is a very significant probability that instability could have occurred without erosion and piping. However, given the very high probability of erosion, it seems likely that both mechanisms were involved in the failure.

Design analyses

The design was divided into five reaches, designated as Reaches I, II, III, IV, and V. The south and north breaches both occurred in Reach III, which encompassed Stations 37+00 to 120+00. Seepage analyses described in paragraphs 44, 45, 47, and 52 of the geotechnical investigation report[3] were performed to evaluate the potential for erosion and piping in areas where the London Avenue Canal levee and I-wall were underlain by sand, as at the south and north breach locations. The analyses were performed using flow nets, Lane's Weighted Creep Ratio method[4], and Harr's Method.[5]

Flow net analyses were performed for the levees in Reach IV and Reach V, based on levee base width of 80 ft, 60 ft depth of pervious foundation soil, and canal water level at 10.2 ft NAVD88. The calculated values of exit gradient were found to be about 0.25. These were judged to provide a factor of safety of approximately 4.0 against erosion and piping. This factor of safety was considered acceptable, and not to require measures to cut off underseepage.

Lane's Weighted Creep Ratio values were computed for the I-walls in Reaches I, II, III, IV, and V. The results indicated that the calculated creep ratios were not acceptable for parts of Reach V where the levee and I-wall would be underlain by sand, according to Lane's empirical criteria. The required cutoff depths within this reach were subsequently evaluated using Harr's Method, and were found to require sheetpile wall penetration to elevation -14.4 ft NAVD88.

None of the seepage analyses considered the possibility that a crack might develop due to water pressures on the I-wall, resulting in flow down the canal side of the wall and into the foundation at that location.

Paragraph 45 of the design report[3] discussed the likelihood that the canal bottom would be covered with silt, which would impede seepage into the foundation in areas where the foundation soils were permeable sand. The relatively short duration of the design high water was also discussed. Based on data from field piezometer studies, it was judged that head levels on the land side of the levee would not be above the ground surface. Paragraph 46 of the report recommended that piezometers be installed and monitored periodically to provide a basis for estimating piezometric levels during floods more accurately, and for evaluating the need for

[3] Geotechnical Investigation, Orleans Levee District, London Avenue Outfall Canal, OLB Project No. 2049-0269, New Orleans, Louisiana, Volume 1, for The Board of Levee Commissioners of the Orleans Levee District, New Orleans, Louisiana, by Eustis Engineering Company, Metairie, Louisiana, 4 March, 1986, contained in GDM86, Volume 1, Part 1, U. S. Army Corps of Engineers, New Orleans District.

[4] Lane, E. W. (1935), "Security from under-seepage – masonry dams on earth foundations," ASCE Transactions, Vol. 100, pp. 1235-1251.

[5] Harr, M. E. (1966), *Groundwater and Seepage*, McGraw-Hill, New York, 381 pp.

landside pressure relief measures. Paragraph 47 of the report discussed the possible consequences of dredging the canal, exposing more pervious materials in the canal bottom, which could result in more adverse seepage conditions, and requested notification if dredging was planned.

Stability analyses performed for Reach III did not show the failure surface entering the sand layer. All of the analyses were performed using slip surfaces within the clay layer beneath the levee and the I-wall. A minimum factor of safety of 1.30 computed by the Method of Planes[6] was required. Required depths of penetration and bending moment capacity for the I-wall were determined by cantilever analyses, as described in paragraphs 48 and 49 of the report[3].

Summary

The analyses described in the preceding sections indicate a strong likelihood that high uplift pressure on the base of the levee and the marsh layer was a key factor in the failures at both the south and the north breaches on the London Avenue canal. At both locations these high uplift pressures probably resulted in development of a rupture through the marsh layer, and hydraulic gradients large enough to cause erosion of the sand.

At the south breach area this erosion may have been the principal mode of failure, with gross instability occurring after considerable volumes of sand, marsh and levee fill had been removed by erosion and piping. Without alteration of the south breach cross section by erosion and piping, the calculated factors of safety with respect to instability are greater than 1.0, indicating that alteration of the profile by erosion and piping probably played an essential role in the failure at this location where the sand was dense, and the sand friction angle would have been high. An additional important factor is that cold-rolled sheetpiles, with weak interlocks, were used at this location. Loss of interlocks during driving in the dense sand would have resulted in even more severe seepage conditions than are reflected in the analyses described here, which modeled the sheetpiles as an intact seepage barrier. The south breach failure appears to have been caused principally by erosion and piping in a localized area focused in a relatively small zone where hydraulic gradients were increased by a rupture through the marsh layer overlying the sand, or by a gap in the sheetpiles due to interlock failure during driving, or both. The conclusion that the failure probably started in a small zone of intense seepage is consistent with the narrow breach that eventually developed.

At the north breach area the probability of erosion and piping is slightly less than at the south breach, although still very high. The probability of instability is higher than the probability of erosion, due to the fact that the sand was loose, and would have had a low friction angle. High uplift pressures likely resulted in a rupture through the marsh layer and the underlying lacustrine clay. At this location, however, the high pore pressures within the sand would be sufficient to cause instability without significant alteration of the cross section by erosion. The failure at the north affected a much wider zone than the failure at the south, indicating that intense localized erosion and piping did not play a key role in the failure at the north breach. It appears that high uplift pressures and lower friction angle of the less-dense sand were key elements in the failure at the north breach.

[6] A study of the Method of Planes, undertaken by IPET at the request of the New Orleans District Task Force Guardian, indicates that the Method of Planes gives lower factors of safety than more accurate methods of analysis, such as Spencer's method. The magnitude of the difference between the two varies from case to case.

Table 1. Hydraulic boundary conditions for seepage analyses
London Avenue south breach

Case	Canal water level – CWL (NAVD88)	Warrington Drive water level – LWL (NAVD88)
1	7.1 ft	-8.4 ft
2	8.2 ft	-8.4 ft
3	7.1 ft	-5.1 ft
4	8.2 ft	-5.1 ft

Table 2. Calculated hydraulic gradients and factors of safety against erosion – London Avenue south breach

Case	CWL	LWL	i = vertical hydraulic gradient	$F_{ersosion} = i_{crit}/i$
1	7.1 ft	-8.4 ft	1.03	0.89
2	8.2 ft	-8.4 ft	1.14	0.81
3	7.1 ft	-5.1 ft	1.13	0.81
4	8.2 ft	-5.1 ft	1.24	0.74

Note: with γ_{sat} = 120 pcf, i_{crit} = 0.92

Table 3. Calculated probabilities of erosion – London Avenue south breach

Case	CWL	LWL	$F_{erosion}$	ΔF	σ_F	F_{MLV}	COV_F	$p_{erosion}$
1	7.1 ft	-8.4 ft	0.89	0.08	0.04	0.85	5%	> 99%
3	7.1 ft	-5.1 ft	0.81					
2	8.2 ft	-8.4 ft	0.81	0.07	0.04	0.78	4%	> 99%
4	8.2 ft	-5.1 ft	0.74					

Notes:
ΔF = change in F due to variation in parameter values
σ_F = standard deviation of factor of safety for the variations considered
F_{MLV} = most likely value of factor of safety
COV_F = coefficient of variation of factor of safety
$p_{erosion}$ = probability of erosion

Table 4. Factor of safety against instability – London south breach

Case	CWL	LWL	$F_{stability}$
1	7.1 ft	-8.4 ft	1.56
2	8.2 ft	-8.4 ft	1.29
3	7.1 ft	-5.1 ft	1.44
4	8.2 ft	-5.1 ft	1.19
5	9.7 ft	-8.4 ft	1.00

Table 5. Probability of instability – London south breach

Case	CWL (ft)	LWL (ft)	ϕ' (deg)	S_u (psf)	F	ΔF	σ_F	F_{MLV}	COV_F	$p_{instability}$
1	7.1	-8.4	40	300	1.56	0.12	0.25	1.50	17%	1%
3	7.1	-5.1	40	300	1.44					
1a	7.1	-8.4	44	300	1.78	0.40				
1b	7.1	-8.4	36	300	1.38					
1c	7.1	-8.4	40	200	1.42	0.28				
1d	7.1	-8.4	40	400	1.70					
2	8.2	-8.4	40	300	1.29	0.10	0.20	1.24	16%	10%
4	8.2	-5.1	40	300	1.19					
2a	8.2	-8.4	44	300	1.47	0.30				
2b	8.2	-8.4	36	300	1.17					
2c	8.2	-8.4	40	200	1.17	0.24				
2d	8.2	-8.4	40	400	1.41					

Notes:
ΔF = change in F due to variation in parameters for the two conditions
σ_F = standard deviation of factor of safety for the variations considered
F_{MLV} = most likely value of factor of safety
COV_F = coefficient of variation of factor of safety
$p_{instability}$ = probability of instability

Table 6. Hydraulic boundary conditions for seepage analyses
London Avenue north breach

Case	Canal water level – (CWL) NAVD88	Pratt Drive water level – (LWL) NAVD88
1	8.2 ft	-8.4 ft
2	9.5 ft	-8.4 ft
3	8.2 ft	-3.9 ft
4	9.5 ft	-3.9 ft

Table 7. Calculated hydraulic gradients and factors of safety against erosion – London Avenue north breach

Case	CWL	LWL	i = vertical hydraulic gradient	$F_{ersosion} = i_{crit}/i$
1	8.2 ft	-8.4 ft	0.95	0.88
2	9.5 ft	-8.4 ft	1.08	0.78
3	8.2 ft	-3.9 ft	1.12	0.75
4	9.5 ft	-3.9 ft	1.25	0.67

Note: with γ_{sat} = 115 pcf, i_{crit} = 0.84

Table 8. Calculated probabilities of erosion – London Avenue north breach

Case	CWL	LWL	$F_{erosion}$	ΔF	σ_F	F_{MLV}	COV_F	$p_{erosion}$
1	8.2ft	-8.4 ft	0.88	0.13	0.07	0.82	16%	91%
3	8.2 ft	-3.9 ft	0.75					
2	9.5 ft	-8.4 ft	0.78	0.11	0.06	0.73	15%	99%
4	9.5 ft	-3.9 ft	0.67					

Notes:
ΔF = change in F due to variation in parameters for the two conditions
σ_F = standard deviation of factor of safety for the variations considered
F_{MLV} = most likely value of factor of safety
COV_F = coefficient of variation of factor of safety
$p_{erosion}$ = probability of erosion

Table 9. Factor of safety against instability – London north breach

Case	CWL	LWL	$F_{stability}$
1	8.2 ft	-8.4 ft	0.99
2	9.5 ft	-8.4 ft	0.77
3	8.2 ft	-3.9 ft	0.84
4	9.5 ft	-3.9 ft	0.67
5	8.1 ft	-8.4 ft	1.00

Table 10. Probability of instability – north breach

Case	CWL (ft)	LWL (ft)	ϕ' (deg)	S_u (psf)	F	ΔF	σ_F	F_{MLV}	C_{OVF}	$p_{instability}$
1	8.2	-8.4	32	300	0.99	0.15	0.17	0.92	19%	70%
3	8.2	-3.9	32	300	0.84					
1a	8.2	-8.4	36	300	1.11	0.24				
1b	8.2	-8.4	28	300	0.87					
1c	8.2	-8.4	32	200	0.89	0.20				
1d	8.2	-8.4	32	400	1.09					
2	9.5	-8.4	32	300	0.77	0.10	0.14	0.72	19%	97%
4	9.5	-3.9	32	300	0.67					
2a	9.5	-8.4	36	300	0.87	0.18				
2b	9.5	-8.4	28	300	0.69					
2c	9.5	-8.4	32	200	0.68	0.18				
2d	9.5	-8.4	32	400	0.86					

Notes:

ΔF = change in F due to variation in parameters
σ_F = standard deviation of factor of safety for the variations considered
F_{MLV} = most likely value of factor of safety
COV_F = coefficient of variation of factor of safety
$p_{instability}$ = probability of instability

Figure 1 – The south breach at the London Avenue canal occurred at 6:00 AM to 7:00 AM on August 29, 2005. The breach, on the east side of the canal, was approximately 60 feet wide.

Figure 2 – The north breach at the London Avenue canal occurred at 7:00 AM to 8:00 AM on August 29, 2005. The breach, on the west side of the canal, is approximately 410 feet wide.

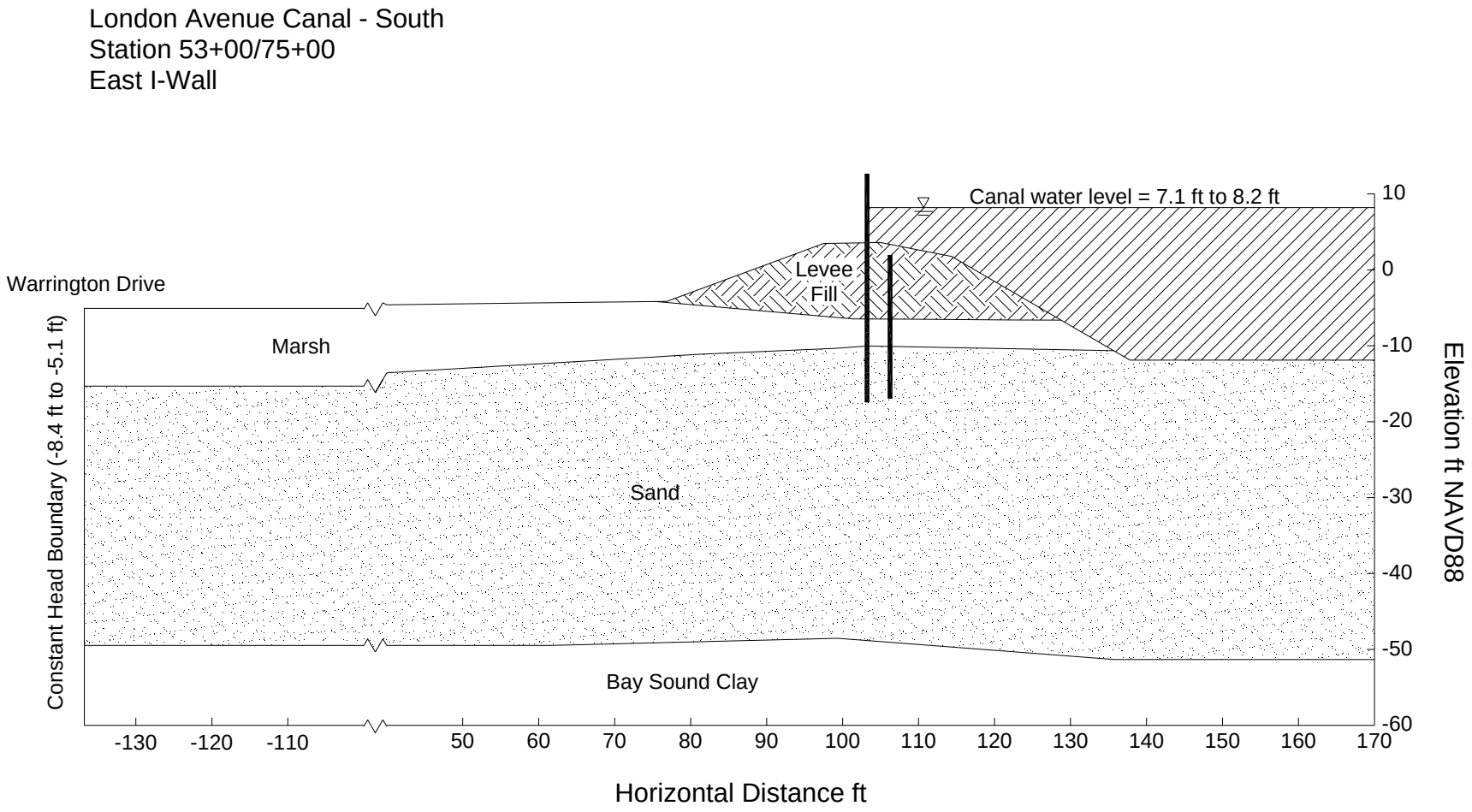

Figure 3 - Schematic cross section at London South breach, with seepage boundary conditions.

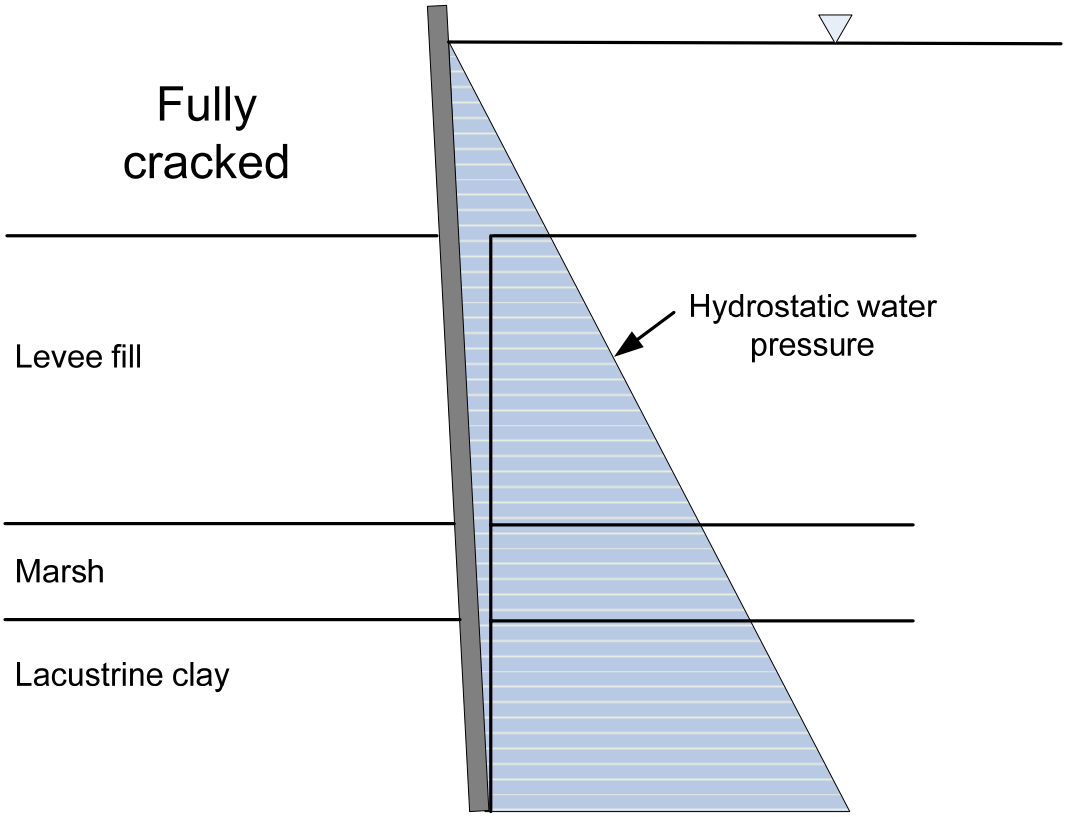

Figure 4 - Schematic of crack used in 17th Street Canal stability analyses.

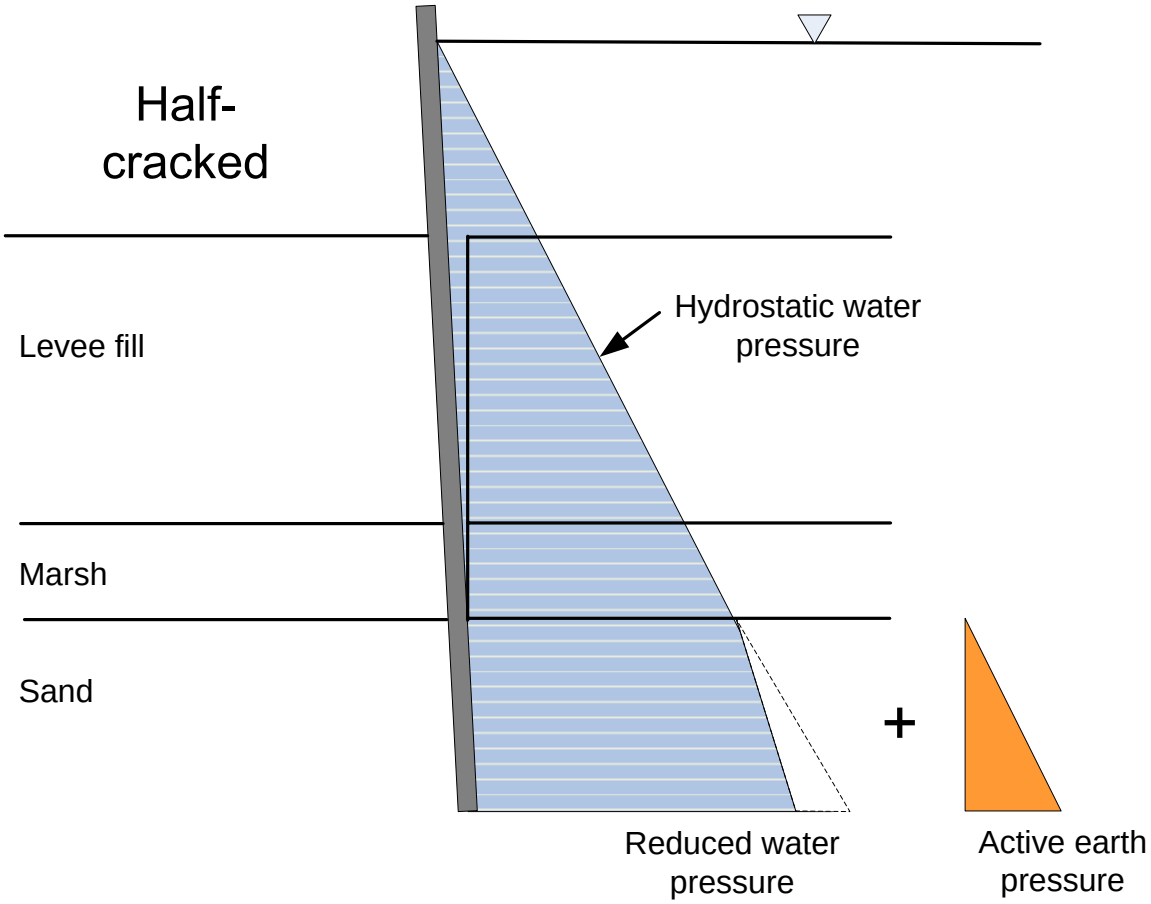

Figure 5 - Schematic of crack used in London Avenue Canal stability analyses.

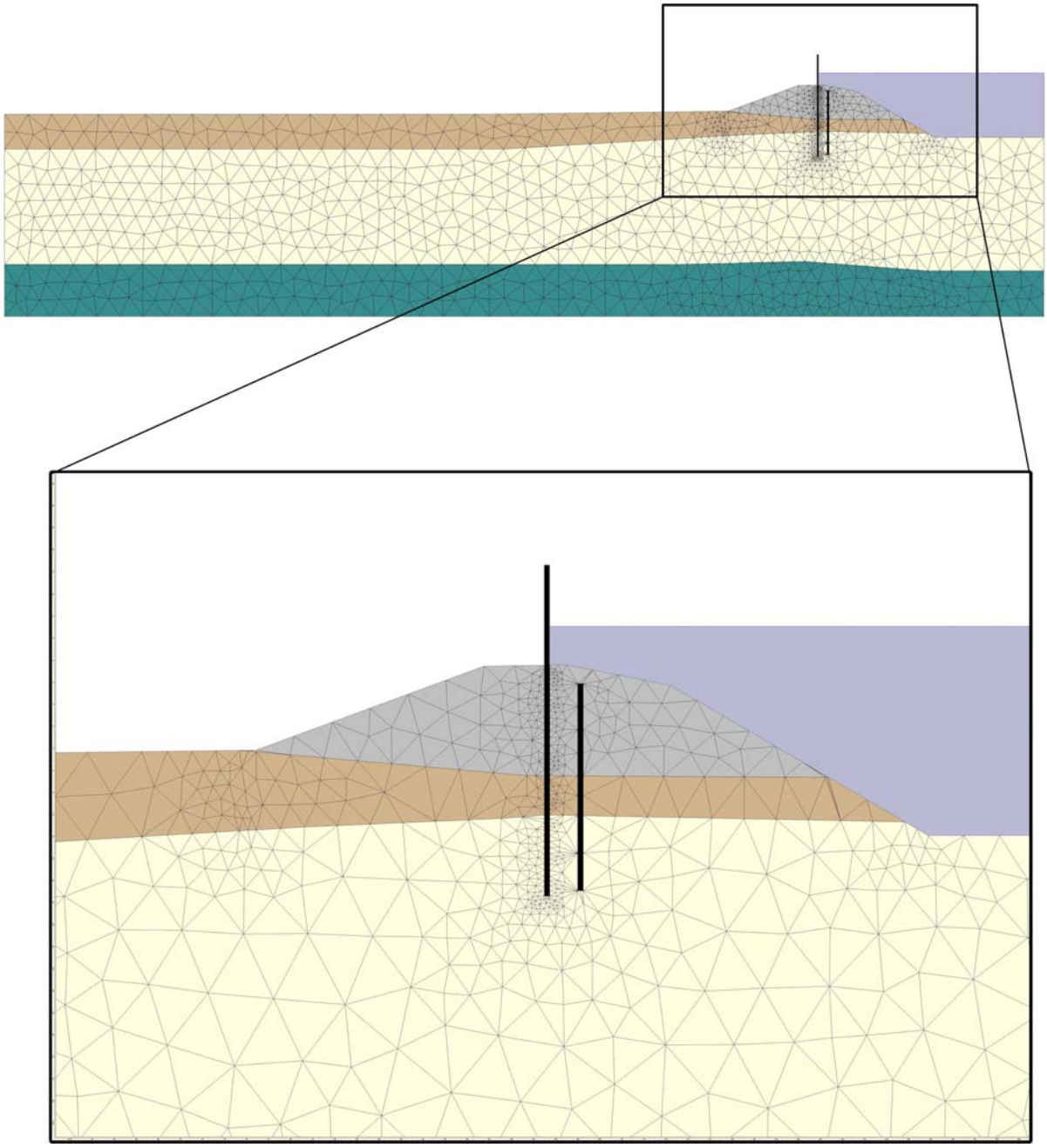

Figure 6 - Finite element mesh used for seepage analysis for London Avenue south breach.

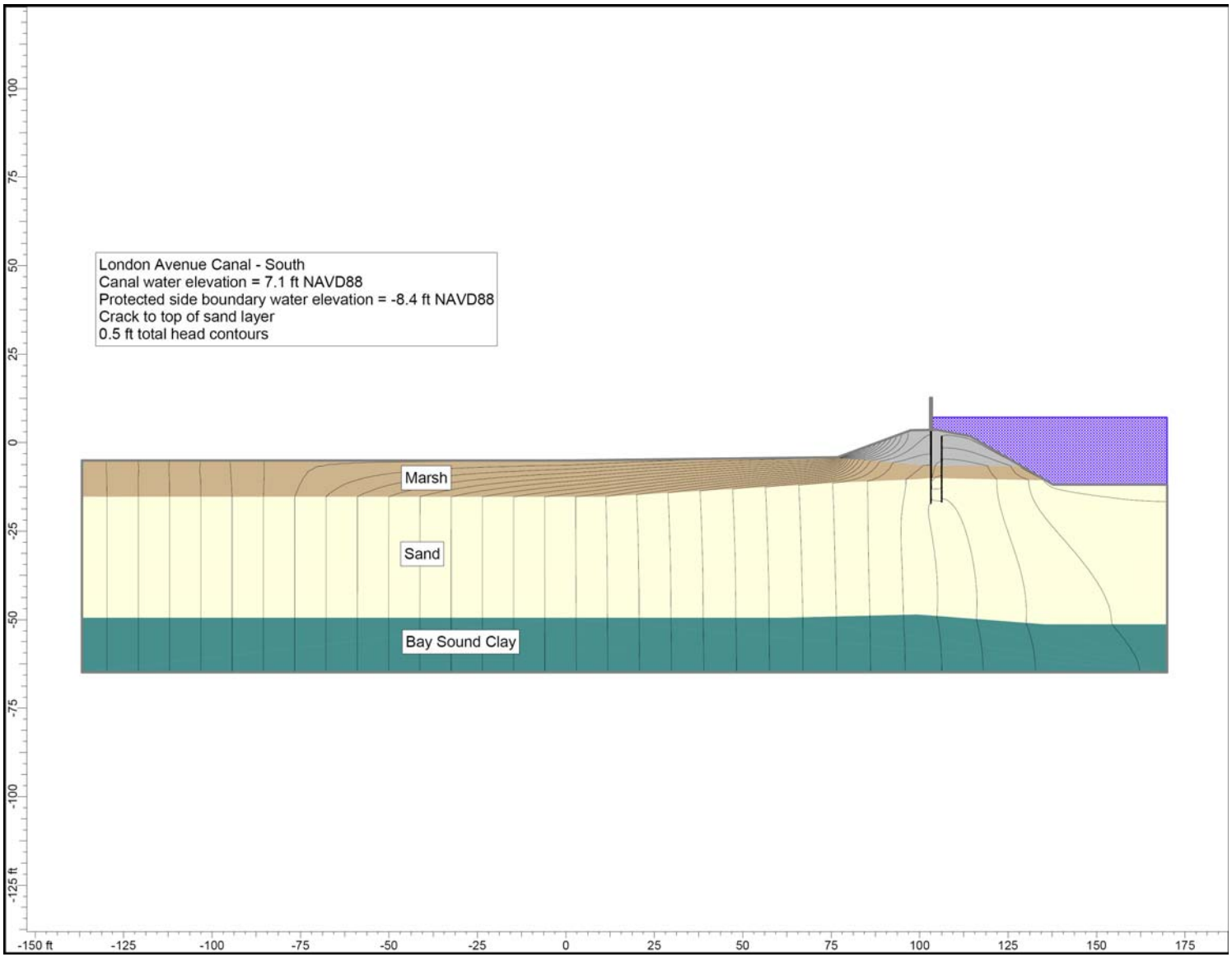

Figure 7 - Total head contours calculated for seepage analysis of London south breach (Case 1).

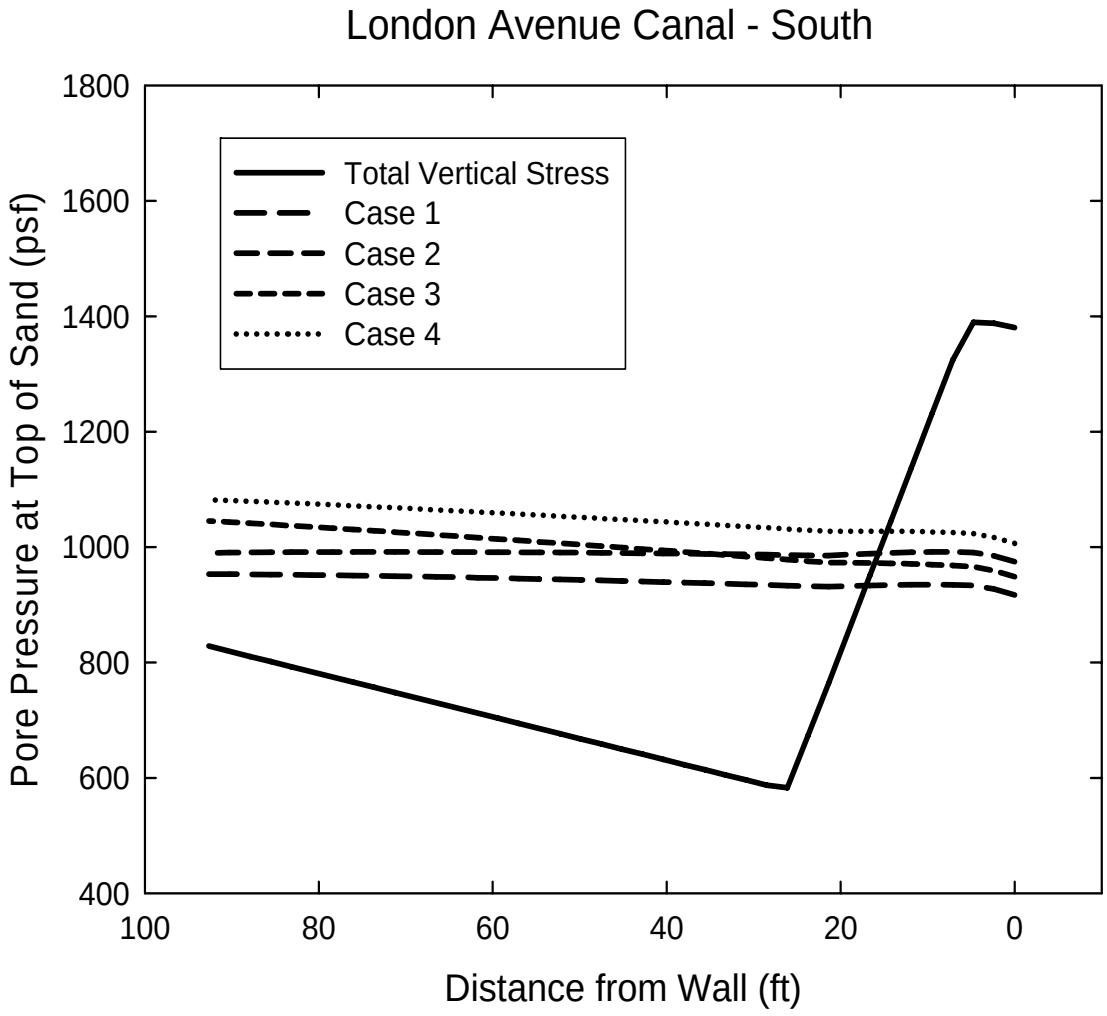

Figure 8 – Calculated uplift pressures and total overburden pressure for London south breach.

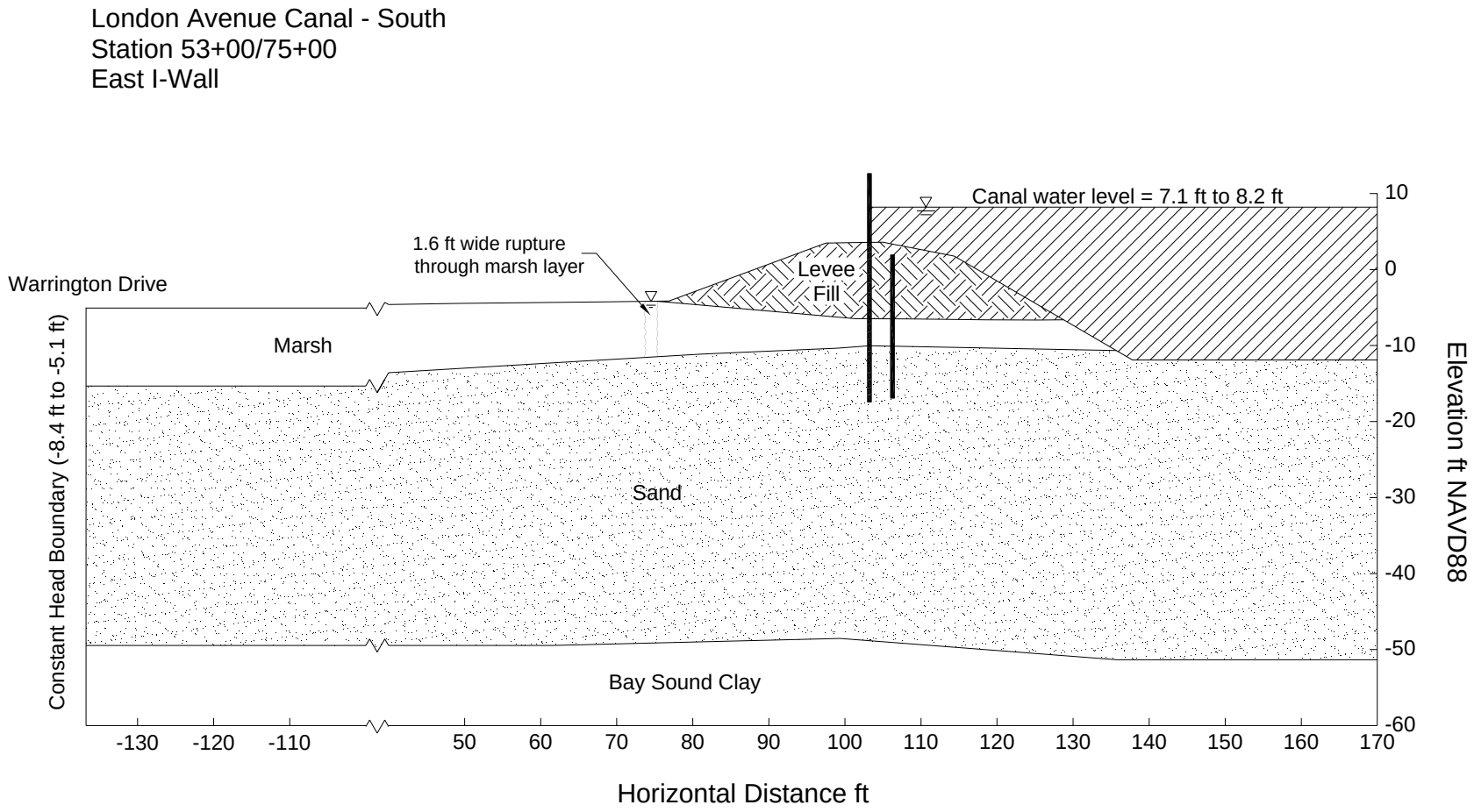

Figure 9 - Schematic cross section at London south breach, showing rupture through marsh layer.

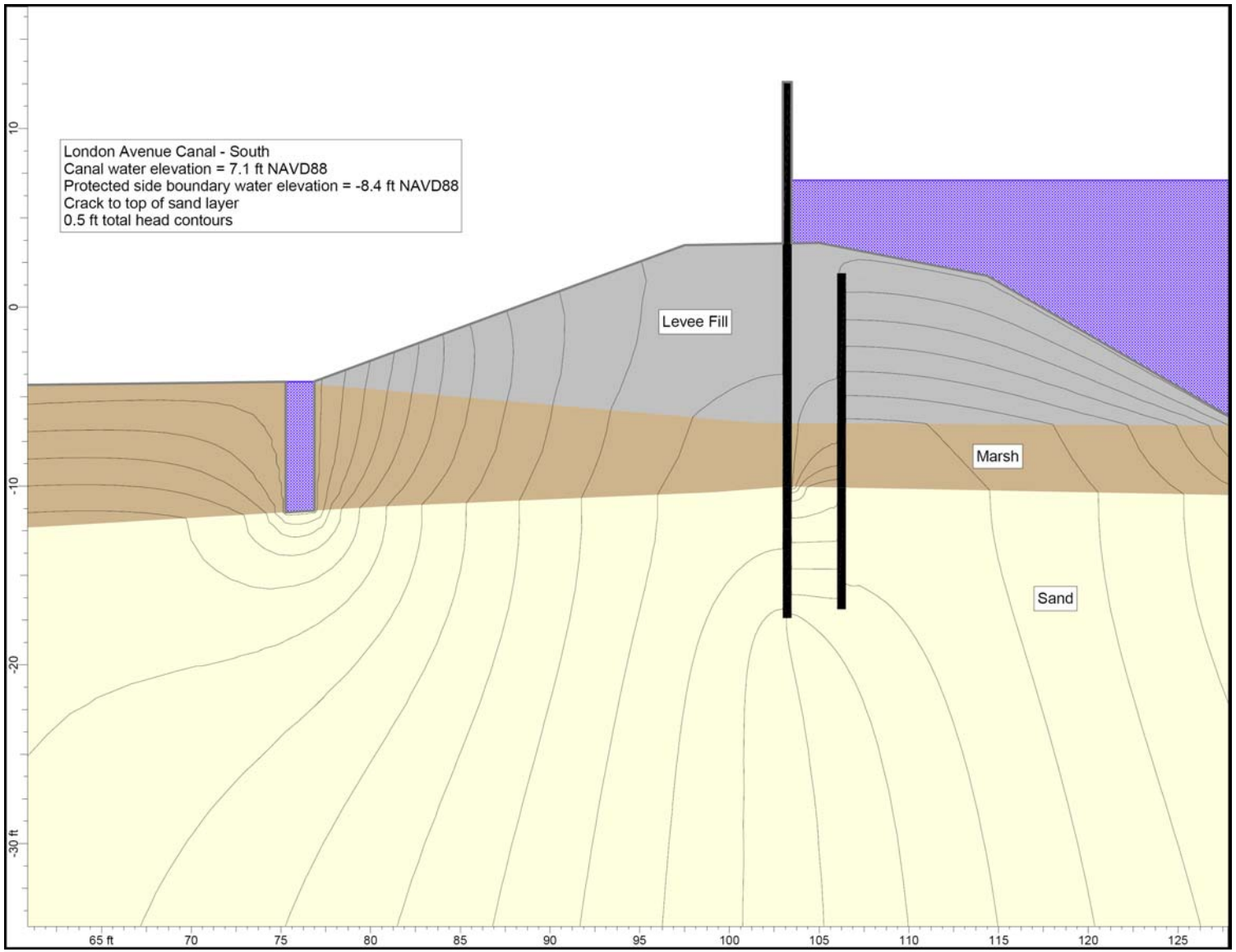

Figure 10 - Total head contours in vicinity of rupture for London south breach.

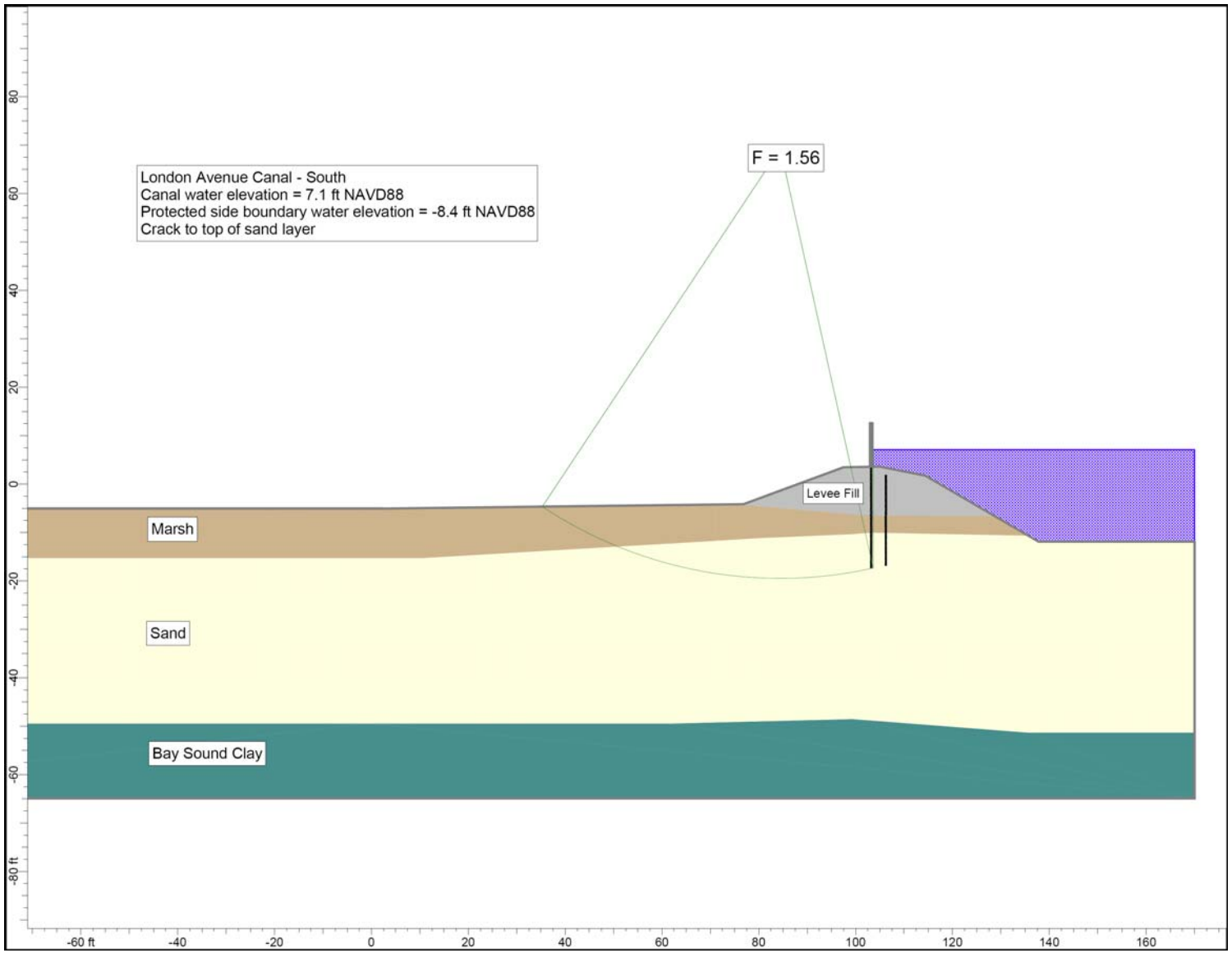

Figure 11 – London south breach Case 1 stability analysis.

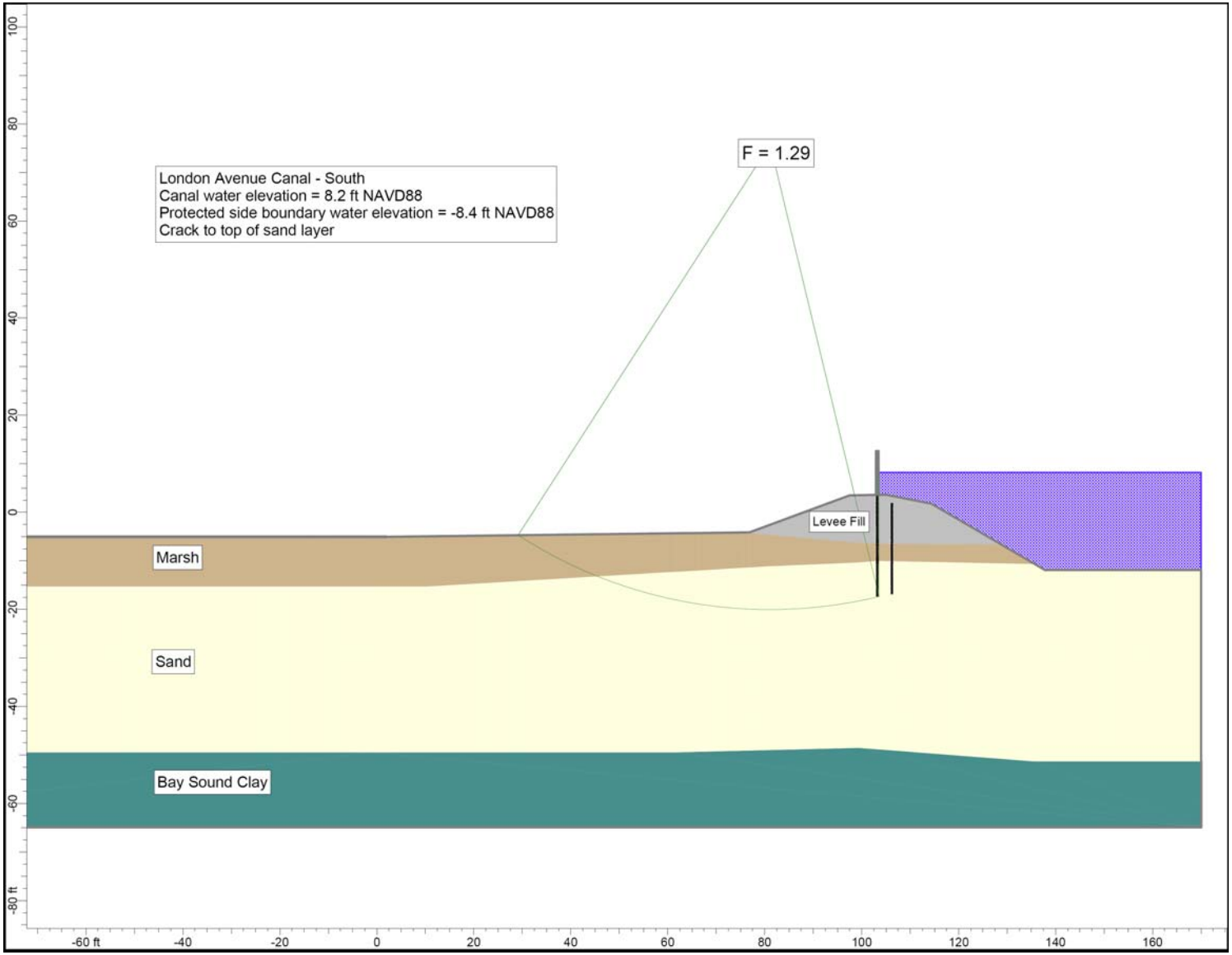

Figure 12 – London south breach Case 2 stability analysis.

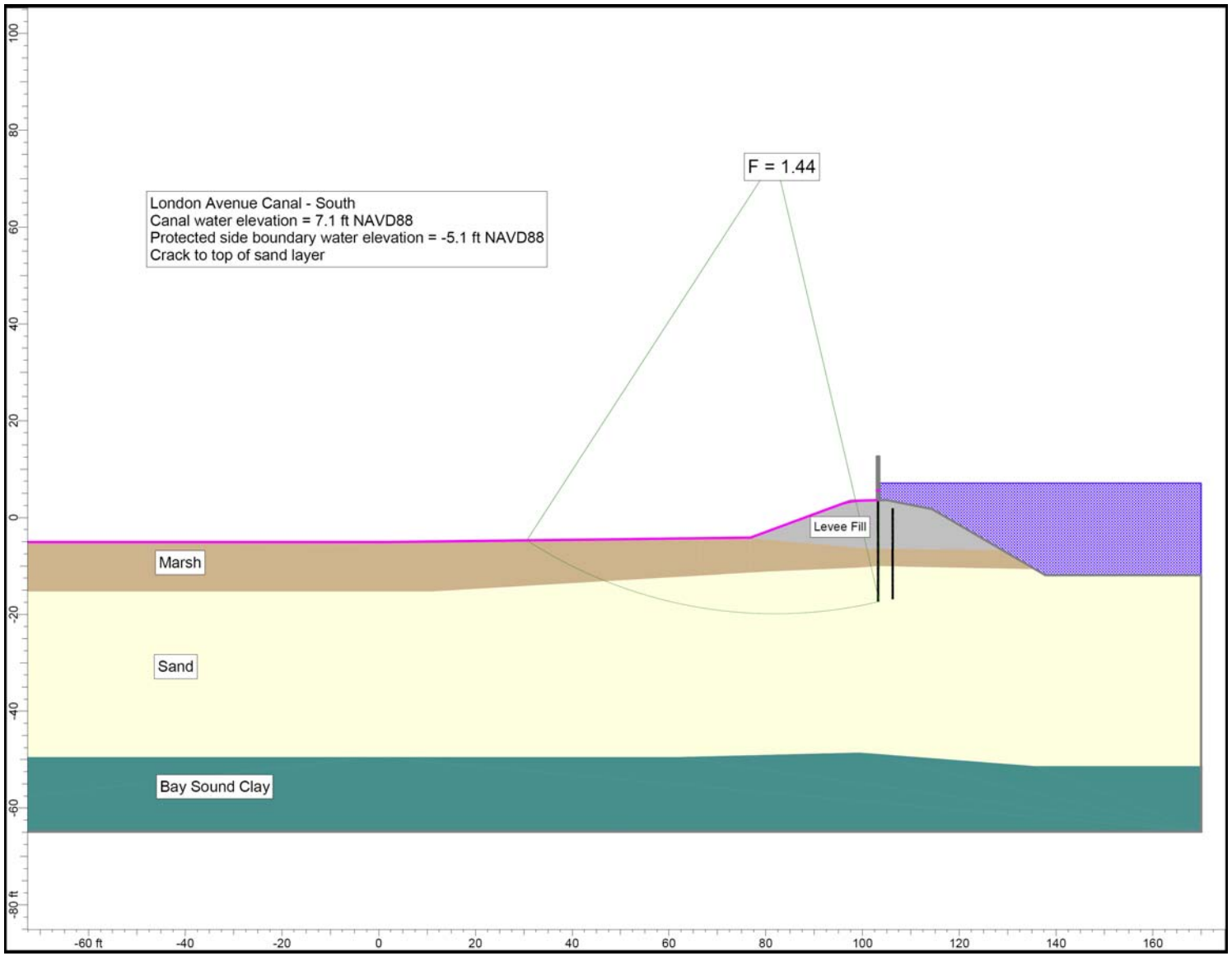

Figure 13 – London south breach Case 3 stability analysis.

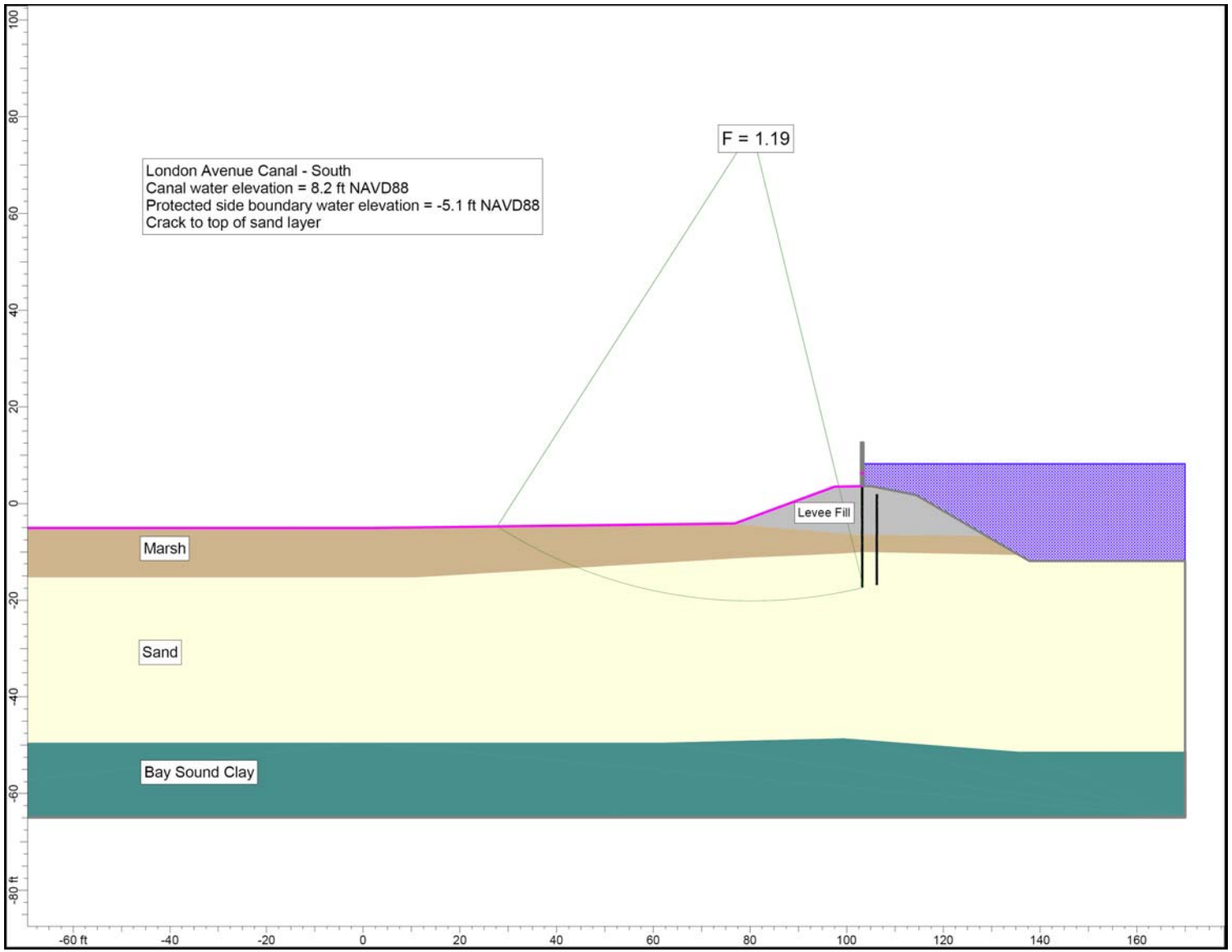

Figure 14 – London south breach Case 4 stability analysis.

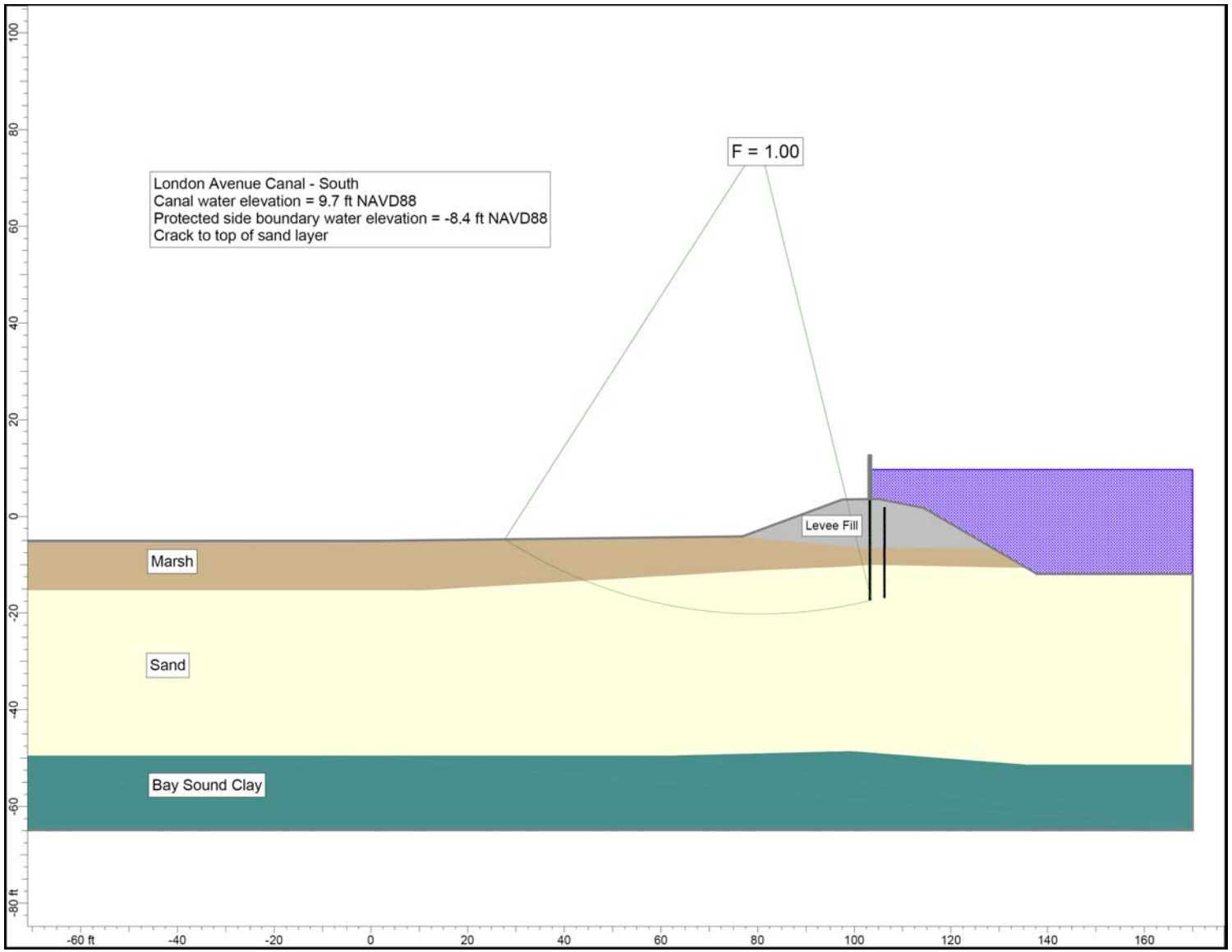

Figure 15 - London south breach Case 5 stability analysis.

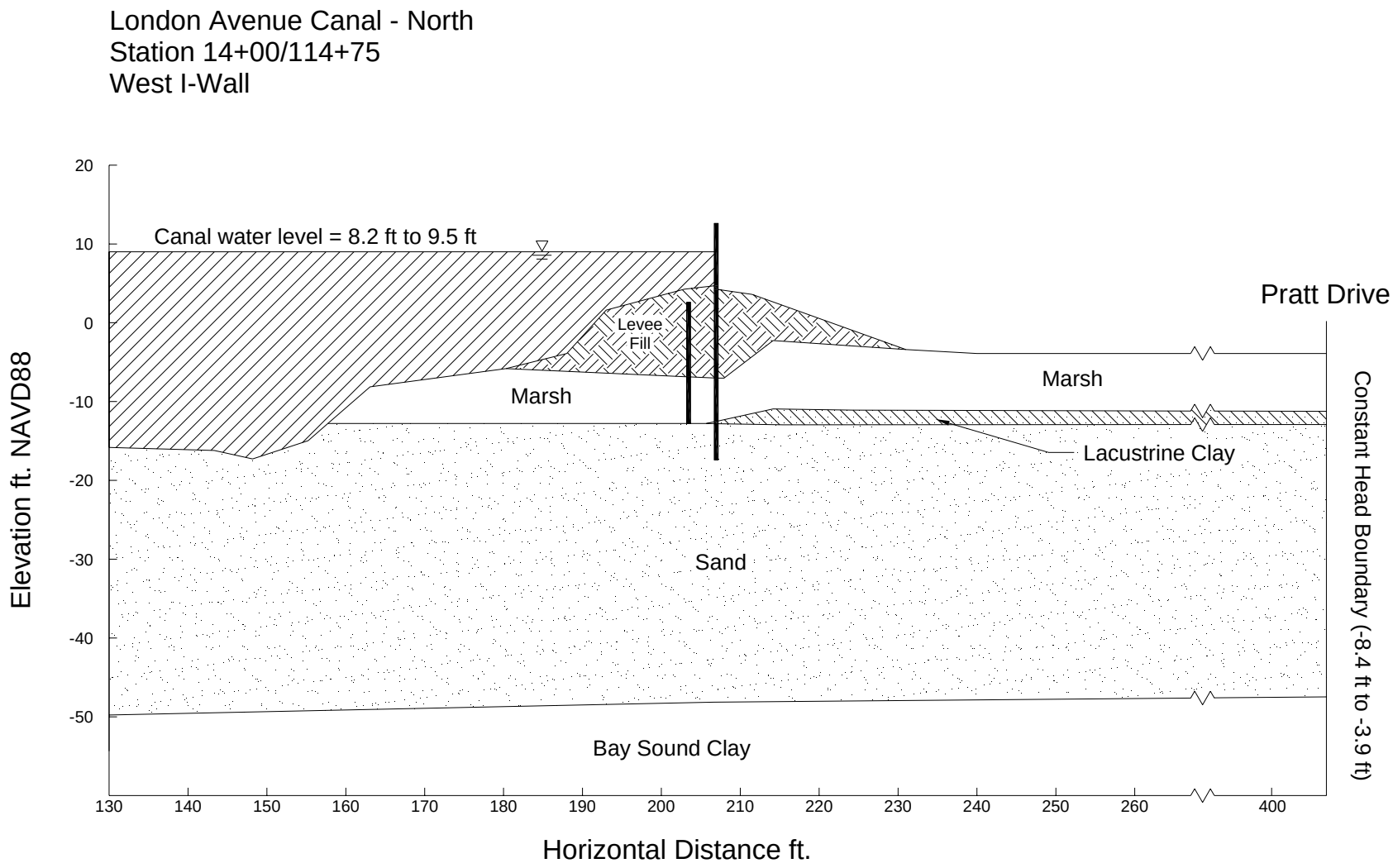

Figure 16 - Schematic cross section at London north breach, with seepage boundary conditions.

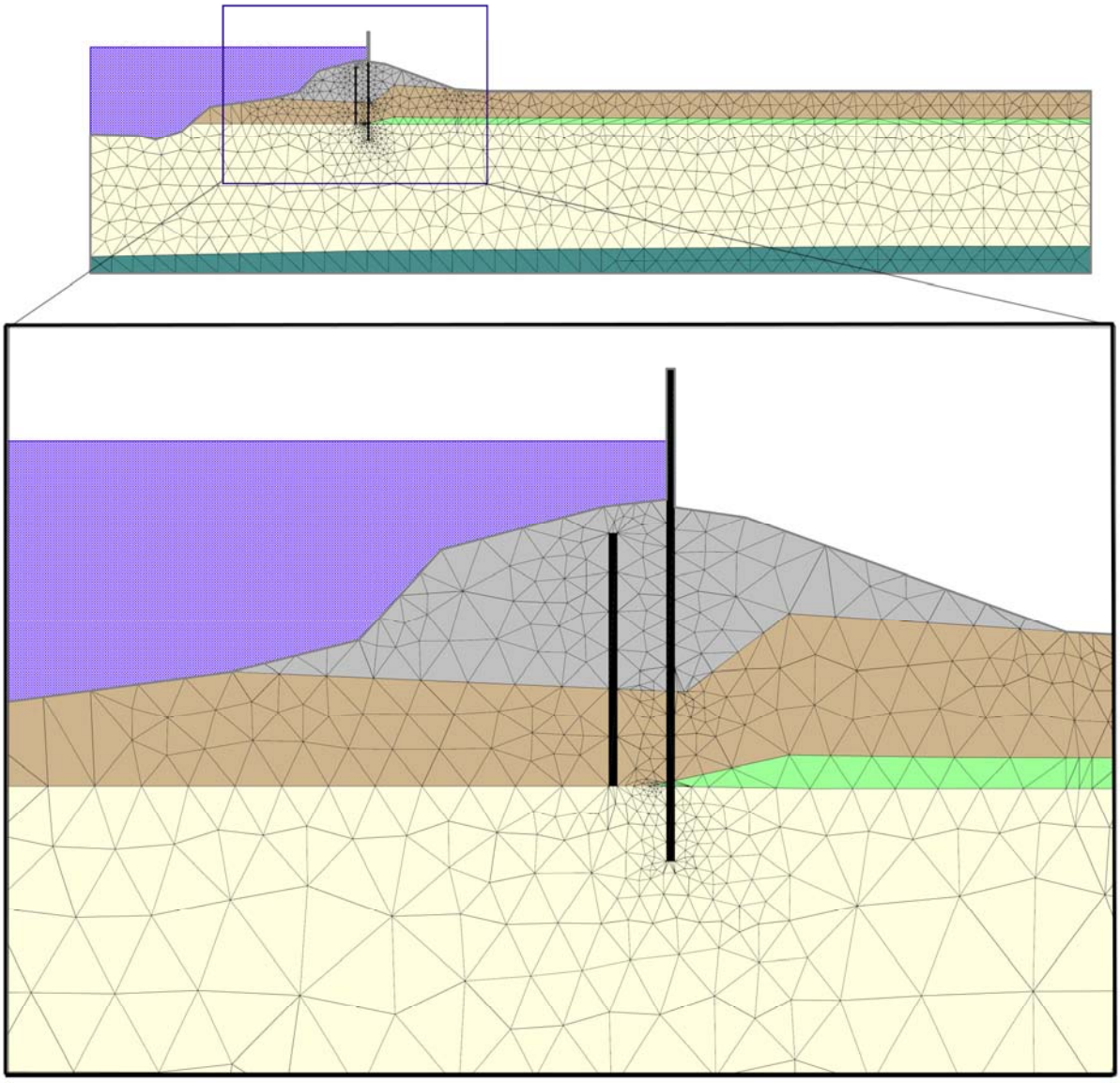

Figure 17 - Finite element mesh used for seepage analysis for London Avenue north breach.

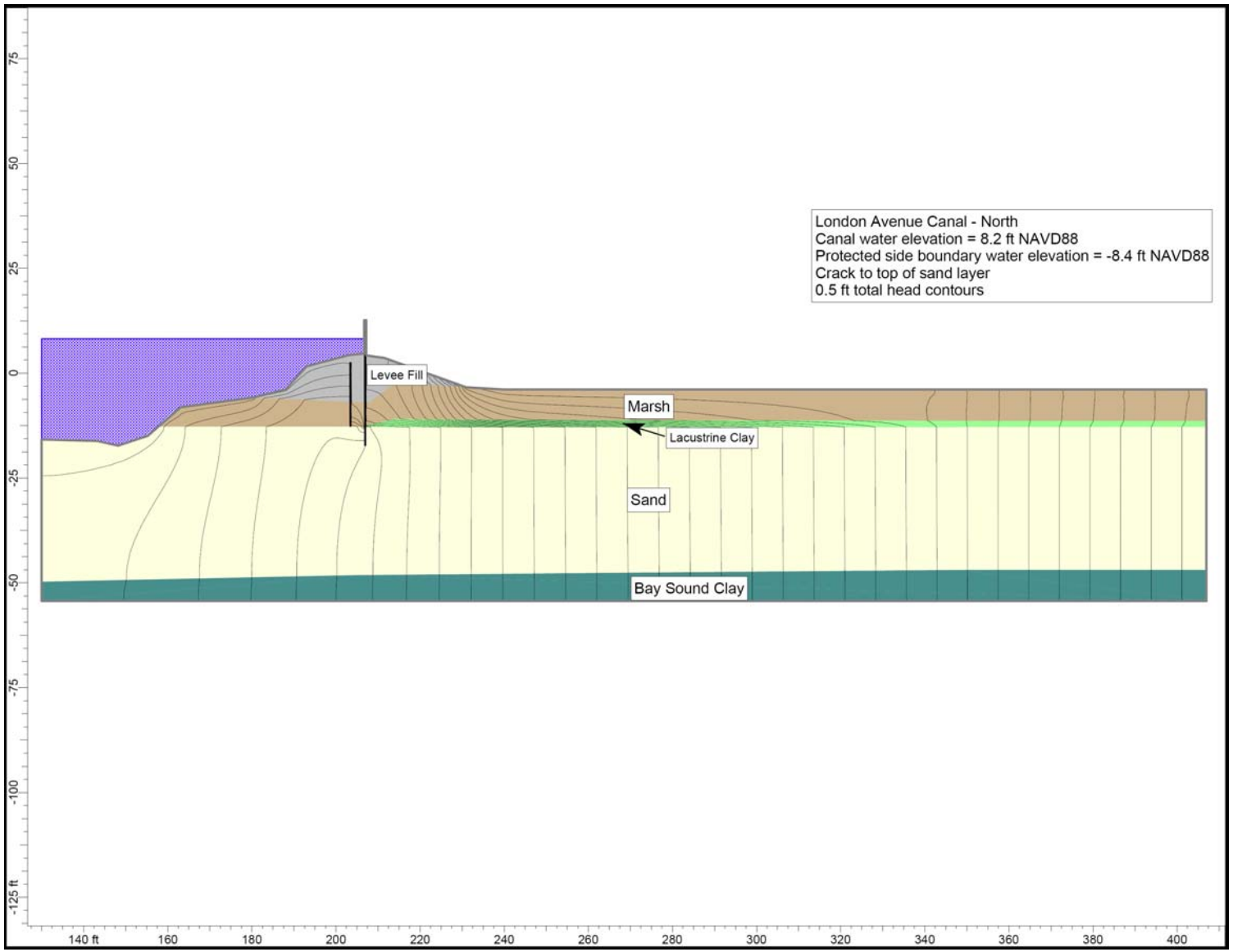

Figure 18 - Total head contours calculated for seepage analysis of London north breach (Case 1).

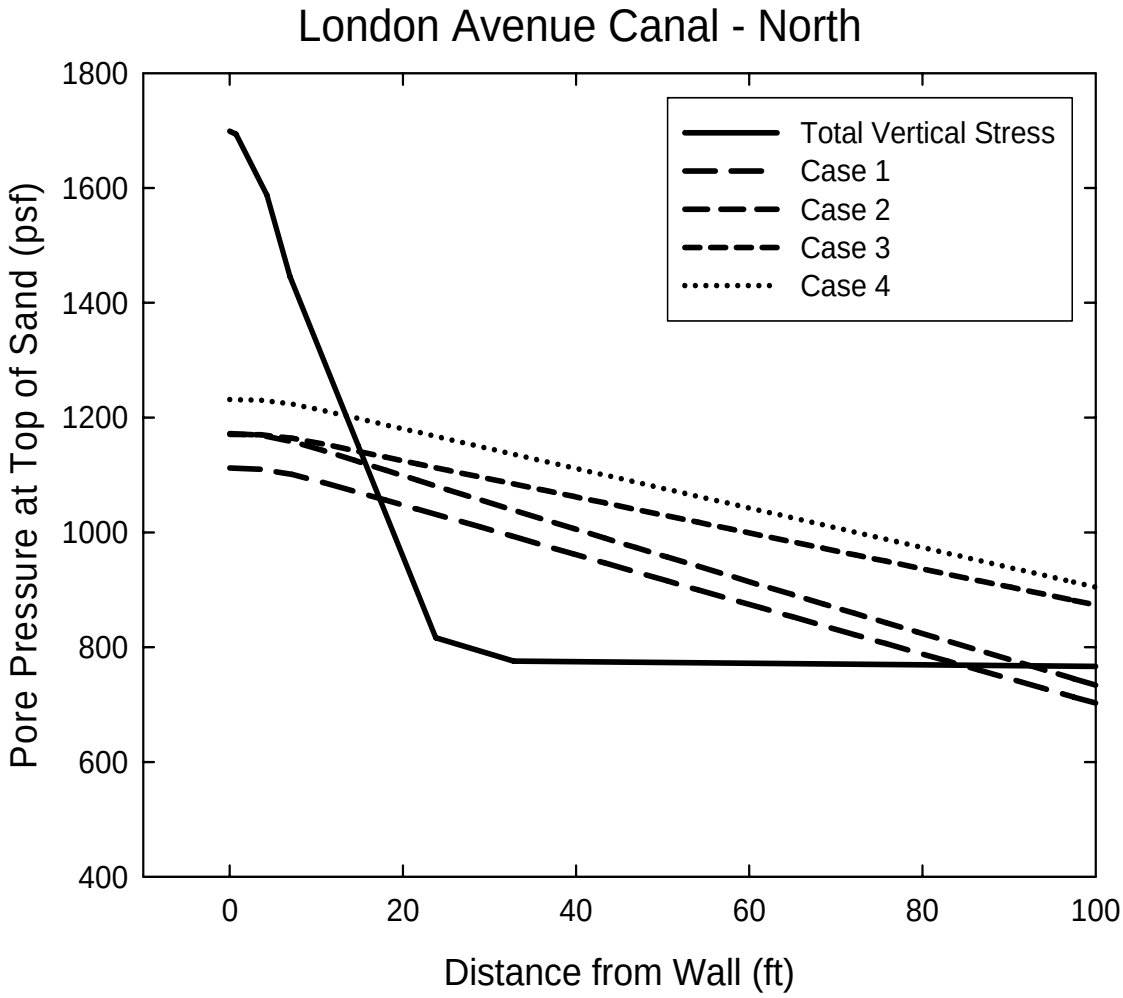

Figure 19 – Calculated uplift pressures and total overburden pressure for London north breach.

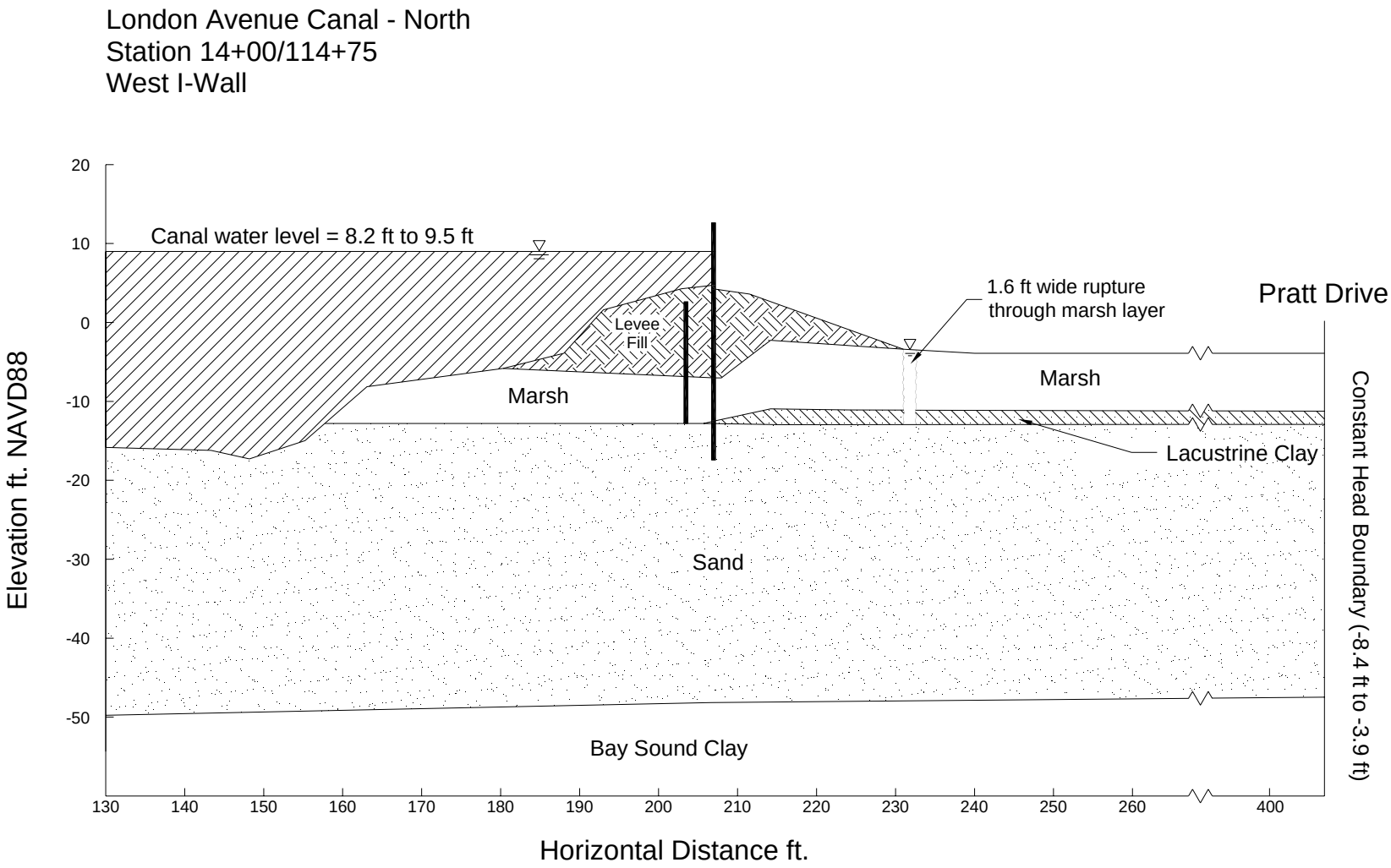

Figure 20 - Schematic cross section at London north breach, showing rupture through marsh layer.

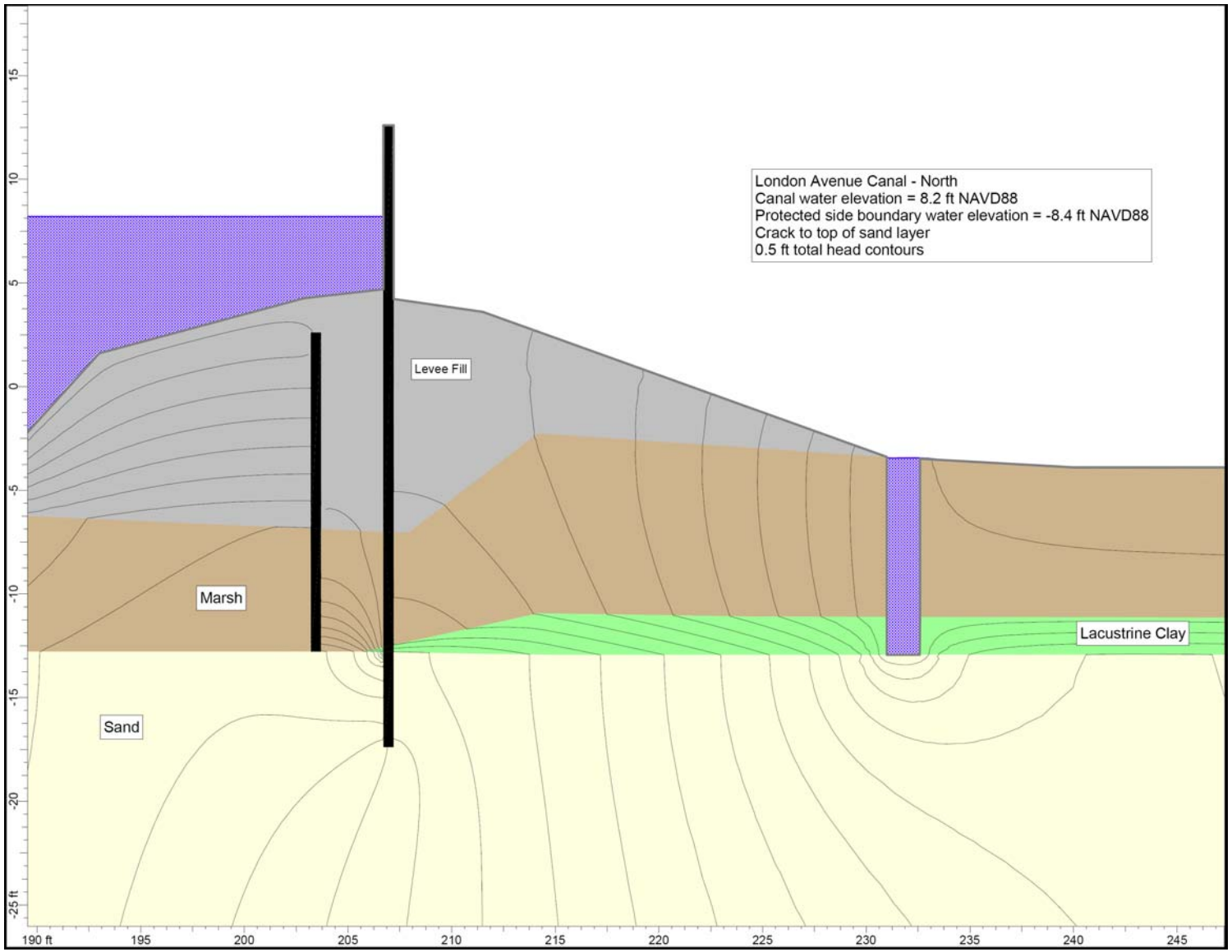

Figure 21 - Total head contours in vicinity of rupture for London north breach.

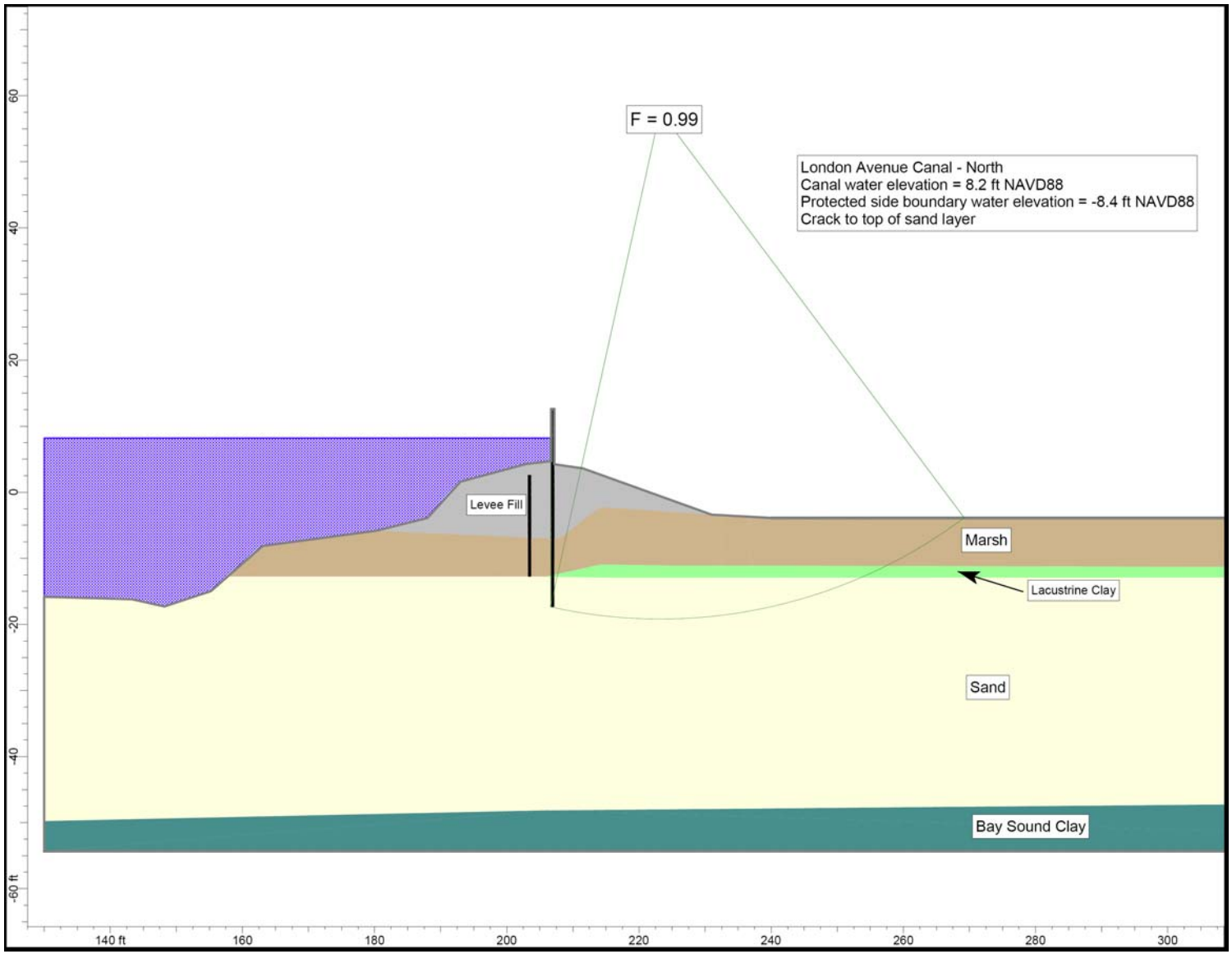

Figure 22 – London north breach Case 1 stability analysis.

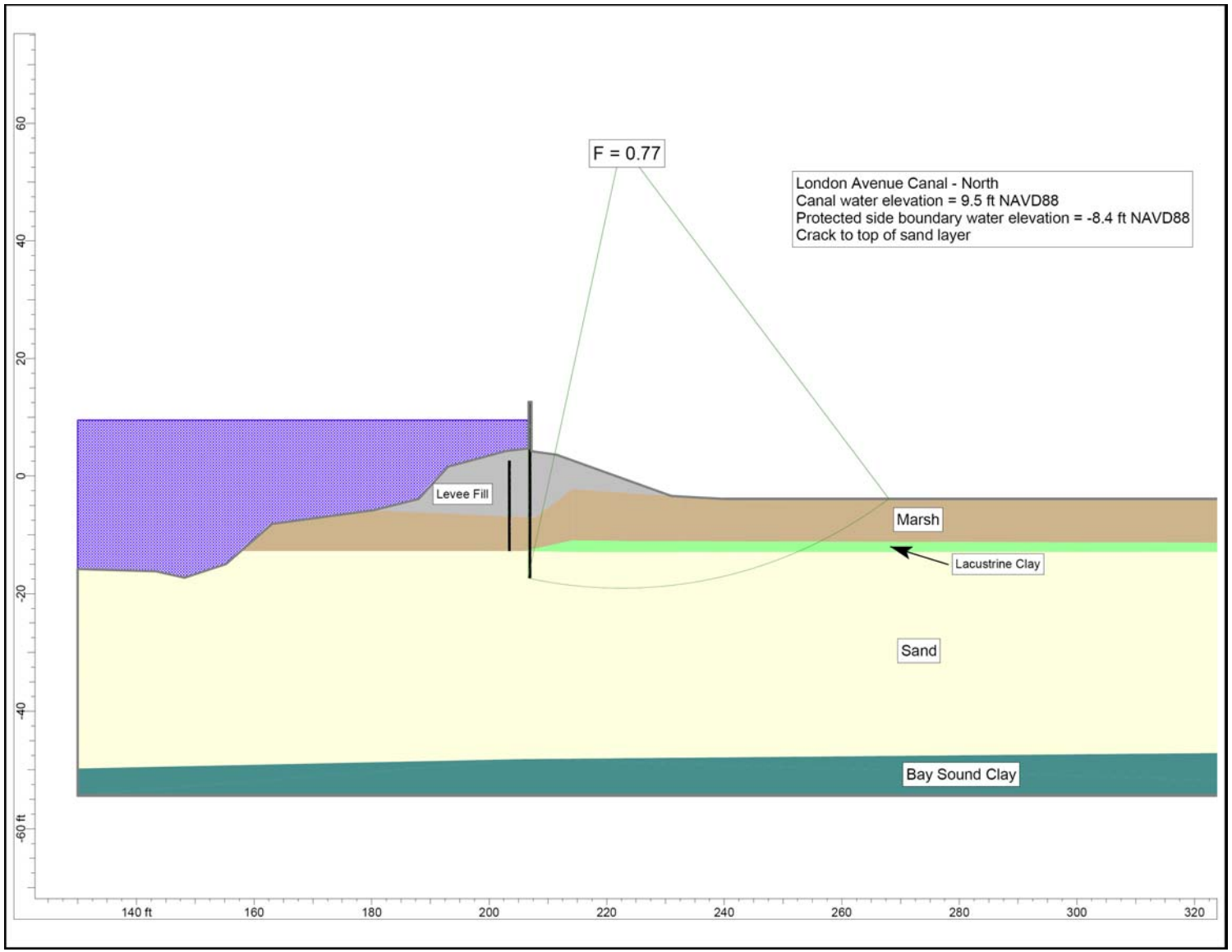

Figure 23 – London north breach Case 2 stability analysis.

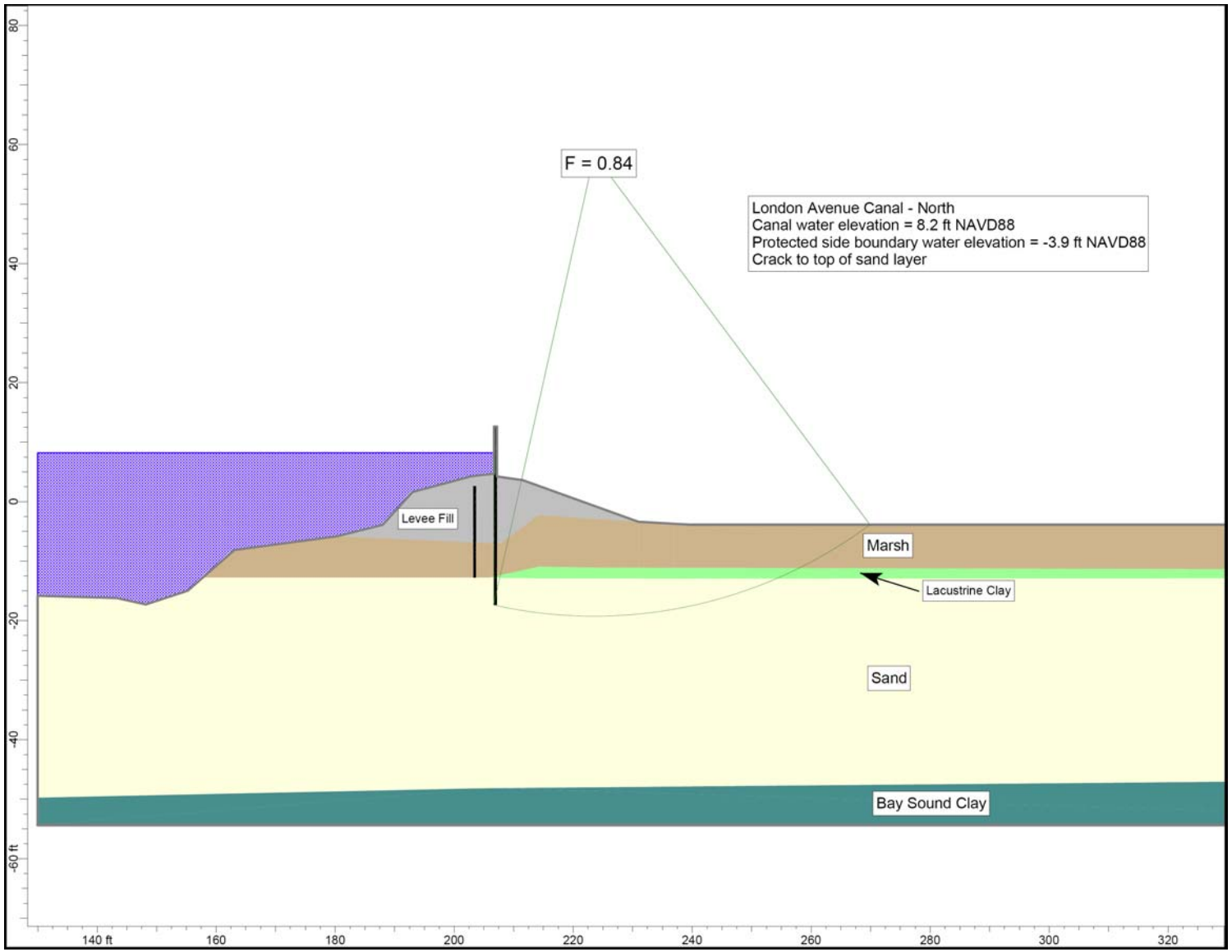

Figure 24 – London north breach Case 3 stability analysis.

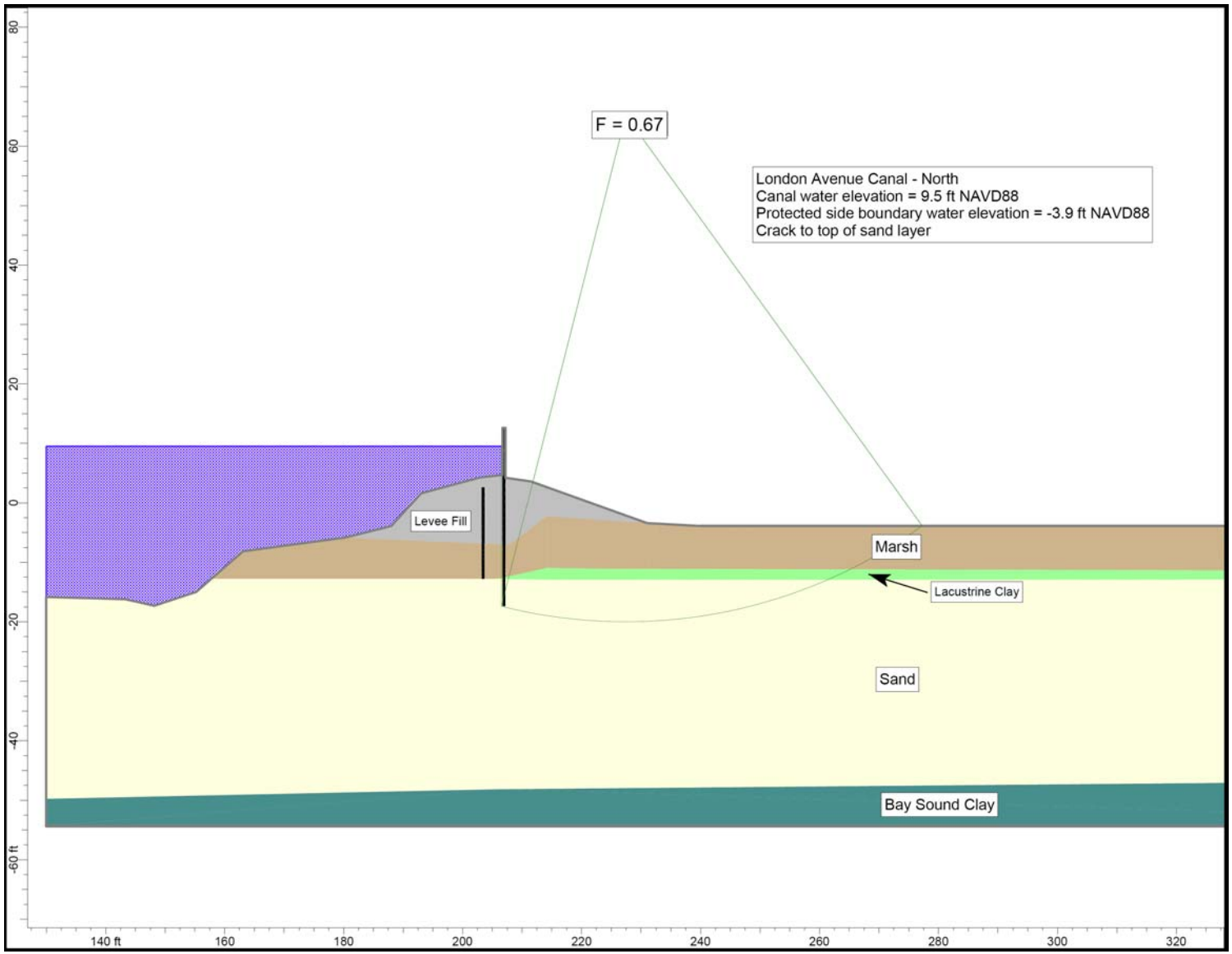

Figure 25 – London north breach Case 4 stability analysis.

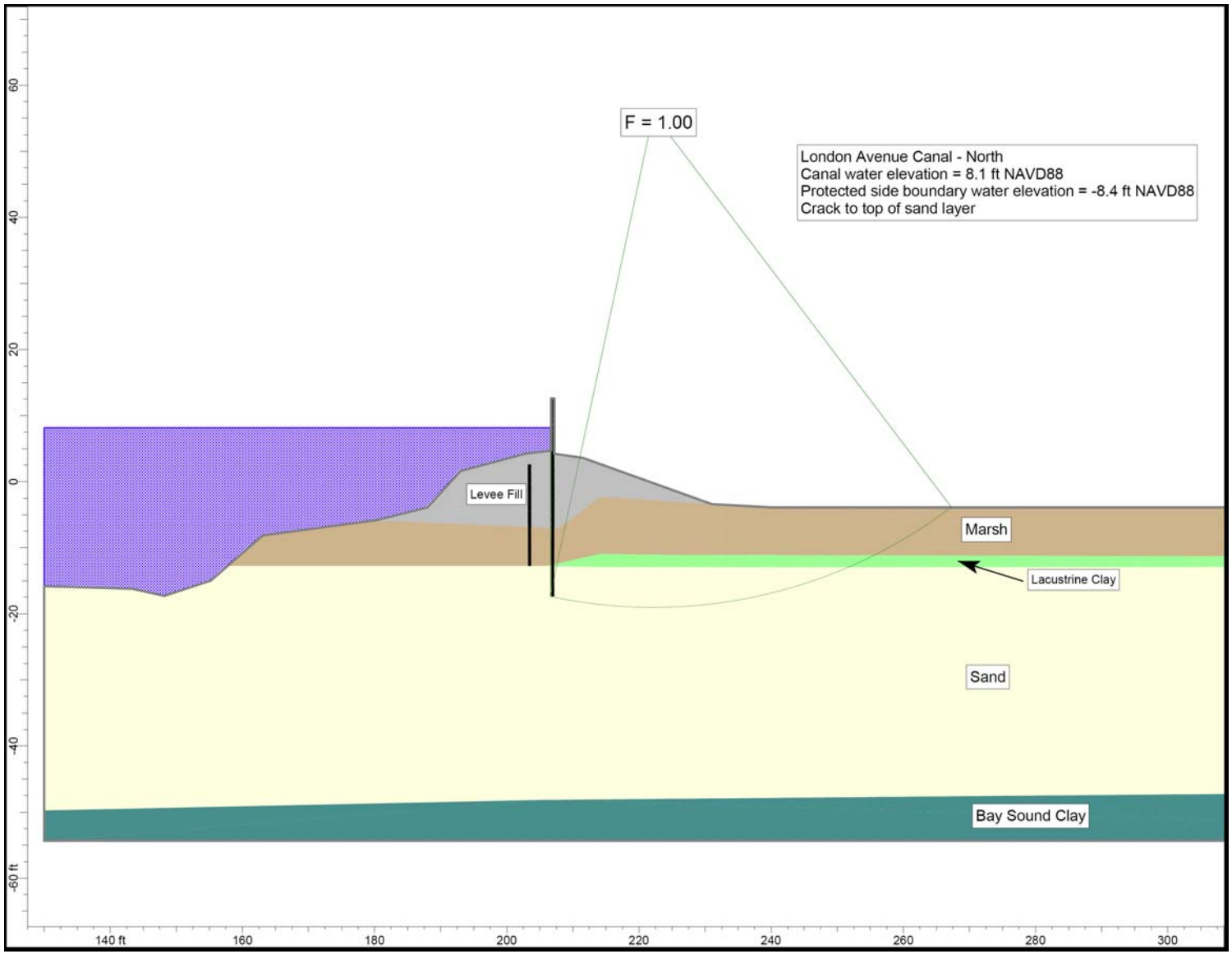

Figure 26 – London north breach Case 5 stability analysis.